Modeling and Experimental investigations of Drilling Carbon Fiber Reinforced Composites

by

Zahra Sadat Fattahi Massoom

A thesis submitted to the
School of Graduate and Postdoctoral Studies in partial
fulfillment of the requirements for the degree of

Doctor of Philosophy in Mechanical Engineering

Faculty of Engineering and Applied Science

University of Ontario Institute of Technology (Ontario Tech University)

Oshawa, Ontario, Canada

April 2021

THESIS EXAMINATION INFORMATION

Submitted by: **Zahra Sadat Fattahi Massoom**

Doctor of Philosophy in Mechanical Engineering

Thesis title:
Analytical, Numerical and Experimental Investigation in Drilling Carbon Fiber Reinforced Composites

An oral defense of this thesis took place on March 2, 2021 in front of the following examining committee:

Examining Committee:

Chair of Examining Committee	Dr. Martin Agelin-Chaab
Research Supervisor	Dr. Hossam Kishawy
Examining Committee Member	Dr. Sayyed Ali Hosseini
Examining Committee Member	Dr. Shaghayegh Bagheri
University Examiner	Dr. Ghaus Rizvi
External Examiner	Dr. Philip Koshy, McMaster University

The above committee determined that the thesis is acceptable in form and content and that a satisfactory knowledge of the field covered by the thesis was demonstrated by the candidate during an oral examination. A signed copy of the Certificate of Approval is available from the School of Graduate and Postdoctoral Studies.

Abstract

The application of composites in different industries especially aerospace industry has significantly increased due to their phenomenal mechanical characteristics. Drilling woven composite parts is one of the most common operations in assembly, and therefore selecting the ideal process parameters and tool geometry is a vital key to control the drilling-caused damages (i.e. delamination). In this study, a novel mathematical model is proposed to predict the critical thrust force at which delamination starts. The model takes into account the thermo-mechanical loads with considering a mixed-mode of fracture that takes place in the delamination area for unidirectional composites. The proposed model has been benchmarked with five previous models including different composite materials, drill bits and feed rates. It was found that the proposed model offered the highest average accuracy among all studied cases. This model explains how the delamination area starts with a circular cross-sectional area in the entrance layer and grows into an ellipsoid, in the same direction of the fibers, in the exit layer. In addition, the visualization of this phenomena is executed through Finite Element Analysis. Furthermore, the second phase of this work offers an integrated approach to fully understand the machining process of woven composites. This integrated approach includes three stages; (i) experimental investigation of drilling thrust force, (ii) investigating the importance of drill bit geometry, and (iii) Effects of feed rate scheduling on minimizing delamination. It was perceived that only scheduling the feed rate is not sufficient for minimizing the delamination. However, updating the chisel edge ratio based on the drill bit geometry results in predicting a more accurate thrust force which can sufficiently minimize the delamination. Finally, the results obtained in this work provide a valuable guideline to better utilize common machining tools and resources while maintaining the quality of drilled holes.

Keywords: Delamination, feed rate scheduling, woven composites, drilling, critical thrust force

AUTHOR'S DECLARATION

I hereby declare that this thesis consists of original work of which I have authored. This is a true copy of the thesis, including any required final revisions, as accepted by my examiners.

I authorize the University Of Ontario Institute Of Technology (Ontario Tech University) to lend this thesis to other institutions or individuals for the purpose of scholarly research. I further authorize University of Ontario Institute of Technology (Ontario Tech University) to reproduce this thesis by photocopying or by other means, in total or in part, at the request of other institutions or individuals for the purpose of scholarly research. I understand that my thesis will be made electronically available to the public.

Zahra Sadat Fattahi Massoom

STATEMENT OF CONTRIBUTIONS

I hereby certify that I am the sole author of this thesis and that no part of this thesis has been published or submitted for publication. I have used standard referencing practices to acknowledge ideas, research techniques, or other materials that belong to others. Furthermore, I hereby certify that I am the sole source of the creative works and/or inventive knowledge described in this thesis.

ACKNOWLEDGEMENTS

To My Beloved Parents, Dr. G. Alavi and Dr. S. H. Fattahi Massoom

I would like to express my special gratitude to my supervisor, Professor H A. Kishawy, for his great support and encouragement to conduct this research. Professor Kishawy's extensive knowledge and significant experience has not only helped me throughout my research but has also allowed me to overcome any obstacles throughout this process.

I would also like to express my sincere appreciation to the members of the supervisory committee for their helpful comments and discussions. I would like to thank my colleagues at the Machining Research Laboratory (MRL) for their continuous support and motivation.

Table of Contents

List of Tables

List of Figures

List of abbreviations and Symbols

E_l	Elasticity in longitude direction
E_t	Elasticity in transverse direction
a, b	Dimensions of the delaminated area
δ	Plate deflection
δ_0	Plate deflection coefficient
q	Distributed load
W	Total work done by thrust force
U	Total strain energy
U_d	Energy absorbed by the delaminated part
P	Total thrust force
P_c	Point load portion of the thrust force
P_L	Distributed portion of the thrust force
D_{ij}	Stiffness matrix components
G_I	I mode of fracture, rate of the energy release
G_{II}	II mode of fracture, rate of the energy release
G_c	mixed mode of fracture, rate of the energy release
β	B-K criterion value
ζ	B-K criterion value
γ	Chisel edge ratio
α	Thermal expansion coefficient
M_{xx}	Resultant moment/unit length of y coordinate
M_{yy}	Resultant moment/unit length of x coordinate
M_{xy}	Twisting moment by shear stresses perpendicular to the x axis
M^T	Thermal moment
$\varepsilon_x\ \varepsilon_y\ \varepsilon_{xy}$	strain components
$\kappa_x\ \kappa_y\ \kappa_{xy}$	Radii of curvature components
ΔT	Temperature variation

Chapter 1. Introduction

1.1Literature Review

Carbon fiber-reinforced plastics (CFRP) are one of the major groups of composite materials and have a significant role in aerospace, automotive, and civil applications. More specifically lightweight design has gained noticeable importance in the aerospace industry. Approximately 30% of the Boeing 767 outer surface area [1] and 50% of the Boeing 787 main structure includes composites [2]. The purpose of reinforcing plastic resin matrices, like epoxy, is to enhance specific strength, fracture toughness, corrosion resistance, and specific stiffness paired with preferred damping properties.

Mechanical properties of the CFRP and essentially the structure yield point [3] will be different by the size and type of the mentioned damaged area [4]. Similar to a previous study by [5], the deformation becomes easier while the drill bit is exiting the lower plies, especially the bending at the drilled area since the workpiece rigidity has been reduced. In the previous attempts [6], different methods have been introduced to avoid delamination as in [7]. In a recent study for micro-drilling the effect of point angles in energy consumption of the drilling process is investigated. [8]. For step by step drilling. Effect of feed condition has been studied as well in [9] illustrating the correlation of feed rate and thrust force. In [10] the effect of machine parameters such as spindle speed and feed rate are investigated, showcasing how applying nanofiller additives can help to prevent delamination. Although executed on glass fiber composite, the study in [11] emphasizes on measurement and analysis of thrust force and introduces the feed rate as the most significant parameter for process responses. In some cases, a cryogenic drilling environment has been suggested to improve the damaged area [12], [13]. In the recent study [14] thrust force, torque, delamination factor, and

drilled holes diameter were also considered in drilling of CFRP composites under dry, MQL (Minimum Quantity Lubrication) and cryogenic environments and the results were explained and MQL method was found to be the most suitable alternative to dry drilling.

Delamination is among the composite cracking phenomena; Matrix cracking occurs more frequently than fiber fracture, and it is due to the exceeded strength of the matrix. The two main components of matrix cracking are intralaminar cracking (within a ply in the matrix), and interlaminar cracking or delamination (between the nearby plies), [15]. In this research, a perfectly cured composite without any matrix crack or fiber fracture due to inappropriate composite design is under investigation, and delamination is purely caused by drilling.

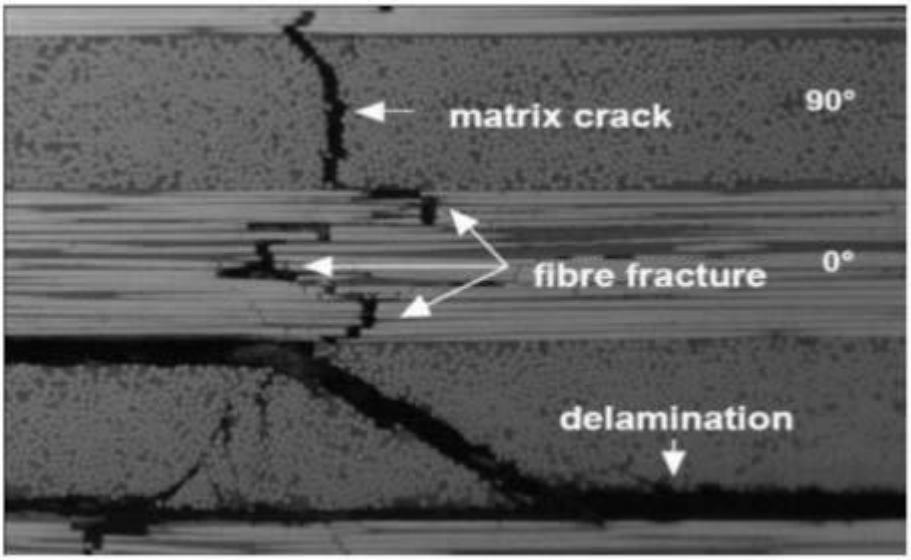

Figure 1-1 Matrix cracking, fiber fracture and delamination [16]

Among all critical design considerations, such as the mechanics of the fiber-reinforced plastics, the tool geometry, feed rate, and drilling thrust force, the thrust force [17] is the most crucial response to determine the quality of the drilled holes. A recent work [18] studied the relationships among the fiber orientation, thrust force, and tool wear and how thrust force is a major contributor in delamination. In [19], [20] the

researchers discussed the possible role of the chisel edge and point angles of the drill bit in cutting orthotropic composites by introducing two semi-empirical coefficients. Table 1-1 Literature review of previous analytical models presents a summary of the most popular previous analytical models.

This research studies a thermo-mechanical model to estimate the critical force and avoid delamination failures. The assumptions of linear elastic fracture mechanics and mixed-mode of fracture are included in this study. Different ellipticity ratios are considered to model the induced delamination area. Furthermore, a center point load along with linearly distributed load is applied in the current proposed model to accurately simulate the thrust force. The current work offers the first attempt in the open literature to model the induced thrust force when machining CFRP with taking into account the following design considerations simoultaneously; the two modes of fracture, thermo-mechanical modeling, different elliptical cross-sectional areas, and a combination of center point load along with the linearly distributed load.

Their unique characteristics (non-homogeneity and abrasive fibers [21]) cause damages such as fiber and matrix de-bonding, delamination, and tool wear [22]. Among all the defects, delamination has been considered as the most significant one and it is the last operation performed on the part. It has been reported up to 60% of the parts are rejected because of delamination [23] since it decreases the composite performance over time by reducing the component fatigue strength.

Different experimental investigations have studied delamination and examined the delamination in fully drilled samples; the comprehensive initiation and propagation process of push-out delamination in the drilling process has not been thoroughly explained yet [24].

Table 1-1 Literature review of previous analytical models

Previous models	Assumptions (delamination area/nature of thrust force)	Proposed analytical model
[1995] Jain and Yang	(Elliptical/point load)	$P = 3\pi \sqrt[4]{\frac{D_{22}}{D_{11}}} \sqrt{2G_{IC}\, D_c^*}$
[2001] Lachaud, F., et al.	(Circular/point load)	$P = 8\pi \sqrt{\frac{2\, G_{IC}\, D}{1 - \frac{D'}{8D}}}$
[2001] Piquet, R., et al.,	(Circular/uniform distributed load)	$P = 8\pi \sqrt{\frac{2\, G_{IC}\, D}{\frac{1}{3} - \frac{D'}{8D}}}$
[2017], Ismail, S., et al.	(Elliptical, Thermal strain point/ uniform distributed load)	$P = 12\pi \sqrt[4]{\frac{D_{22}}{D_{11}}} * * \sqrt{\frac{2D_c^*\,(D' + G_{IC})}{16\,\gamma^2 + 2\,(1-\gamma)^2}}$
[2017], Girot, P., et al.,	(Circular point/ triangular distributed load)	$F_z = \frac{\frac{22}{21}\pi\alpha A a^3 \pm \sqrt{\Delta}}{[12(1-\alpha)^2 + \alpha^2]}$

Many researchers have investigated numerical methods such as the finite element analysis of drilling composite laminates. Phadnis et al. [25] presented a great 3D model thrust forces prediction of drilling in CFRP composite which prompt damages to the workpiece and the reported results are in reasonable agreement with experimental results previously published in the literature. This model includes rotary movement of the drill, cutting the workpiece, and element removal. Feito et al. [26] suggested a abridged model of drilling to envision delamination considering the drill acting like a punch. In the mentioned research computational cost has been reduced in

this model but delamination is marginally over-estimated. Authors [27] introduced a different 3D model of drilling to investigate the influences of drill geometry on delamination. In the mentioned study the researchers utilized a step drill and a twist drill where they established that delamination and other workpiece failings could be excluded by proper selection of step drill geometry.

Ultrasonically assisted drilling (UAD) as a novel drilling method has been discussed as an alternative to drilling composites, such as the effective simulations in [28], [29]. Drilling of composites is dependent on numerous variables, making it a complex process to study. Therefore, experimental procedures for observing the effect of tool geometry damages are hard to accomplish. For that matter, simulating the whole operation in Finite Elements can be a solution to completely study composite failure [30].

In Comparison with unidirectional composites, fabric reinforcement provides easier lay-up and better damage tolerance. In this type of composite, a designed carbon fiber pattern including woven tows is existing in the epoxy matrix. Both fiber and matrix simultaneously bear mechanical loads [31]. There are different types of woven composites such as plain, twill, satin, and basket. A new property of these fabric reinforced composites is drape-ability, which is primarily controlled by the weave style [32]. For instance, twill weaves are more drape-able than plain weave, however, they are less drape-able than satin. Twill composite is also more popular in the aerospace industry.

An investigation to relate between the critical thrust force and the feed rate is crucial. In the following research [13], fuzzy logic is utilized in defining the parameters like thrust force, torque and delamination factor in drilling of CFRP composite. The examination of variance results exposes that drill diameter and feed are the most

substantial parameters for thrust force and torque. Unlike the thrust force, the feed rate is directly controllable in computer numerical control (CNC) machines [33]. Establishing an accurate correlation between the thrust force and feed rate would help to monitor the thrust force via feed rate scheduling to minimize delamination. The purpose of feed rate scheduling is to minimize delamination with the use of standard twist drill bit instead of using brazed diamond drills. Cutting conditions have a major impact on the surface quality of the machined carbon fiber reinforced polymers [34]. As an alternative to feed rate scheduling, other methods such as applying a back-up force or support plates [35] can also be utilized. Thrust force is also a function of the tool geometry and drill bit material. Thus, the effect of the chisel edge width on the total thrust force needs to be thoroughly investigated.

1.2 Industrial Applications

With an increase in composites popularity, an increasing importance is observed on manufacturing laminates in a less time consuming manner and more reasonably priced. While numerous unconventional machining processes such as water-jet cutting, ultrasonic cutting, and laser cutting have been developed to machine composites, traditional machining processes such as milling and drilling continue to be widely in use.

Considering the Airbus A350 aircraft consists of more than 55,000 drilled holes, it is fair to state that drilling is seemingly the most popular machining process used in manufacturing. It is necessary to have in mind, while this type of defect includes only 6% of the entire drilling damages, it usually takes up to 5 hours to repair the delaminated area [36]. CFRPs, comparing to isotropic materials such as metals, can behave entirely different under the drilling process. The most challenging defects of composite

materials are delamination at both the entrance and exit [37] of the drilling area of the workpiece and tool wear.

A study by [38] discussed different methods for minimizing the delamination in drilling processes, such as back-up force, pre-drilled pilot hole and peck drilling. The research illustrates peck drilling to have the outcome of lower delamination damage, thrust force, and hole surface roughness.

In another study by [39], hole making in CFRPs is analyzed with comparison between standard twist drill bits, CVD (chemical vapour deposition) coated diamond drill bit, axial and helical milling. The results indicate coating with CVD diamond did not show any major advantages because of higher cutting edge rounding of the tools. Helical milling process improves the results slightly while increasing the process time, however, may decrease the manual reworking. Desipte slightly better hole quality in helical milling, axial drilling maintains popularity due to simplicity of its process.

Further machining processes such as feed rate scheduling introduced in this study can imporve the quality of the drilled holes while maintaining a simpler process.

1.3 Research Objectives

The primary objective of this thesis is to improve the quality of drilling composites by common machining resources. To achieve this purpose, analytical, numerical, and experimental analyses are conducted. The improvement of the drilling process starts with an accurate prediction of drilling thrust force in analytical modeling. Better analytical demonstration drives to a superior understanding of the material behavior and of the laminate's response to the drilling process .

The material model is expected to be capable of recreating material behaviors known to laminated composites.The numerical investigation illustrates the progression

of the damaged area and also provides a chance to simulate the effect of drill bit geometry on delamination defect. The accuracy of the simulation is trailed by initially studying the material models available in the literature review and recognising prospective areas of improvement to attain the numerical prediction of drilling thrust force as precise as possible.

To move the research from the research environment to industry, experimental studies are conducted on woven composites which are more common in the aerospace industry. As the main objective, a set of experiments are designed to correlate the drilling thrust force to critical feed rate which results in the design of a feed rate scheduling and ultimately a feed rate selection guideline to facilitate delamination-free drilling.

1.4 Thesis Outline

After the introduction chapter, introducing the carbon fiber reinforced polymers and the challenges in drilling such composites, chapter 2 investigated a thorough mathematical model considering the mechanical properties, the material failure, and the accurate drilling thrust force model. This mathematical model later on is compared with previously published models in the introduction. The accurate prediction of the thrust force will help to find ideal machining parameters.

Chapter 3, illustrated the progression of the damaged area with help of Finite Element Analysis. This simulation opens up the chance to study the effect of geometry on the damaged area considering the material failure criteria, cohesive zone elements, and lamina fiber orientation.

Chapter 4 utilizes the analytical model proposed in chapter one to introduce a correlation between the thrust force and the feed rate. At this point, the research has a

practical outcome to improve the machining experience and control delamination with help of scheduling the feed rate based on the composite plate. Furthermore, this chapter presents the result of this method of minimizing delamination with different drill bit sizes and proposes a feed rate guideline for drilling processes. The last chapter is a conclusion and outcome of the research.

Chapter 2. Analytical Modeling of Drilling Unidirectional Composites

2.1 Introduction

Different studies claim that the machining operation causes damages that also affect the structure lifespan [40]. The induced cutting temperature also causes damages that must be accounted for in the stress analysis model. Since high temperature [41] affects the properties of laminate composites, thermo-mechanical deformation modeling is more realistic [42].

Regarding modes of fracture, in most cases [33], assumed delamination failure happens in the pure first mode of fracture. However, realistically, even unidirectional composite structures are exposed to both modes I and II, while crack propagation occurs. Therefore, a mixed-mode I/II and a proportionate critical energy release rate, G_c, should be considered. The crack growth rate to an individual ply number has been expressed by a developed function. The proposed function can show the crack size concerning the initiated ply number [17].

A circular area for the induced crack propagation is mostly assumed by the previous proposed analytical models. This exception can be accurate for quasi-isotropic; however, for the orthotropic composites, the crack would grow faster in the direction of the fibers. In the case of unidirectional composites, supposedly, the delamination area starts as a circular area and grows into a damaged elliptical area in the same direction as the fibers, Figure 2-1. Figure 2-2 illustrates the delamination zone on the unidirectional ply laminate.

2.1.1 Drill bit

A twist drill consists of a chisel edge and cutting lips with spiral flutes, Figure 2-3. The helical flute does not cut as they are used to guides the chips from the drill hole out. The cutting lips are on an offset from the symmetrical axis in the center due to the chisel edge. The thrust force pushing down the drill into the workpeice, and the torque applied to the drill and spindle drive cause the rotation of the drill bit. The mechanics of drilling must be analyzed separately for the chisel and cutting lip region.

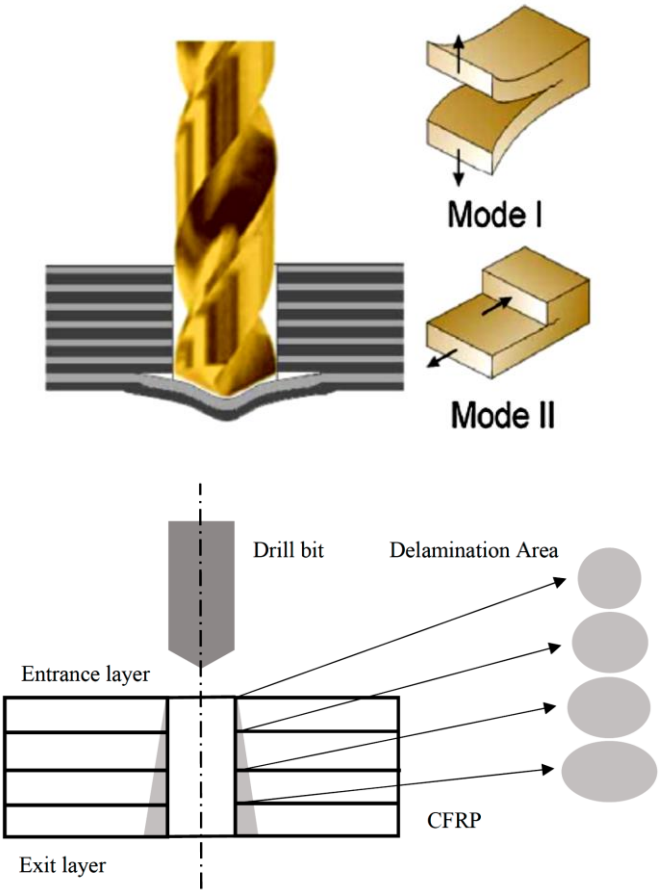

Figure 2-1 (a) Hole exit delamination [36], (b) Delamination area starts as circular and then grows into elliptical

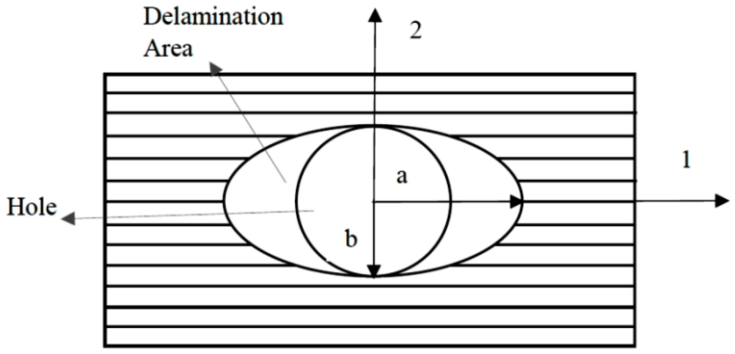

Figure 2-2 Delamination area on the unidirectional ply laminate

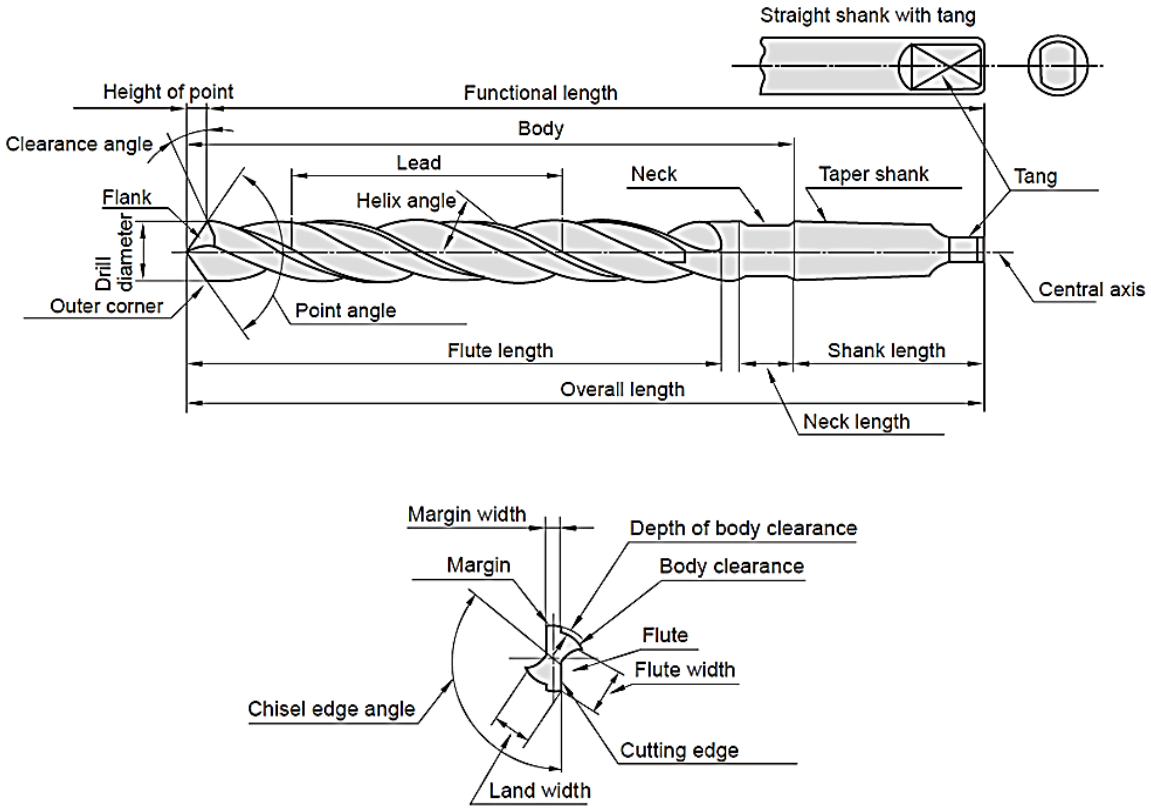

Figure 2-3 Front view and right view of the drill bit [6]

2.1.2 Chisel edge

The chisel edge spreads the material sideward by an indentation mechanism and does not cut. For practical consideration, the chisel forces can be assumed to be about 10-15% more than the lip cutting forces and the torque can be neglected since the chisel width is rather small. This portion of the thrust force is modeled by a center point (punctual) load in the analytical model.

2.1.3 Cutting lip

The geometry of a drill cutting is complicated. The distribution of cutting thrust force is important to be understood on the cutting edges to analytically investigate the critical thrust force. A series of experiments have been done by Girot [36] using Sandvik CoroDrill R846 twist drill suitable for titanium-based alloys and CFRP drilling, Figure 2-4.

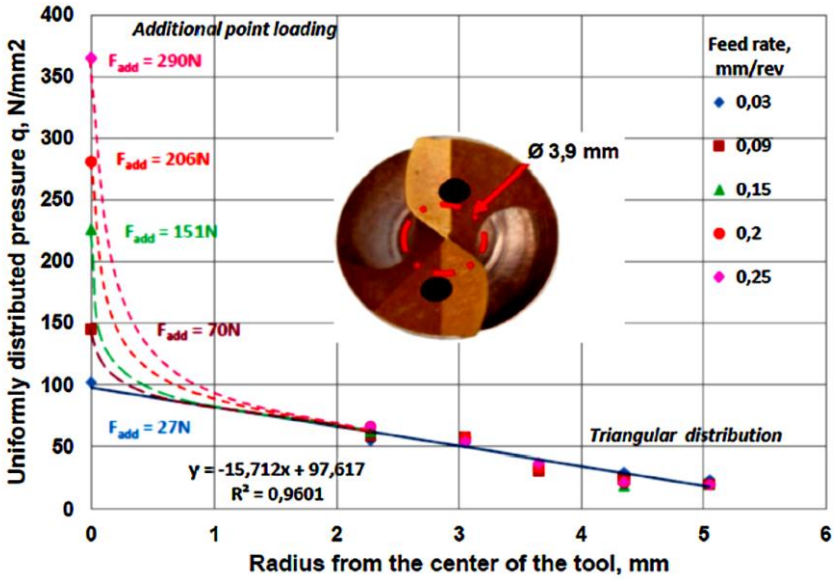

Figure 2-4 Uniformly distributed pressure q of the load [36].

The axial measured load and the uniformly distributed pressure q related to it signifying to the cutting lips clearly show the triangular repartition. As studied, this additional loading is highly dependent on the feed rate.

Here, regarding the laminate theory and fracture mechanics of drilling, a developed analytical model predicts the critical thrust force to minimize and eventually avoid the delamination. The proposed model contributes a better understanding of the delamination occurrence and the thrust force distribution along with the circular growing into the elliptical area. First, the assumptions included in the proposed model are as follows:

• Delamination is considered to have clamped boundary conditions and the circular growing into the elliptical delamination area.

• As the material is carbon/epoxy composite, a brittle material, delamination happens under mixed-mode of fracture and the linear elastic fracture mechanism [43] is applied.

• Point load fragment of the thrust force is modeling the chisel edge force, while a linearly distributed load is modeling the cutting lip force (see Figure 2-5 Point and linear distributed loads in the delamination zone)

• Since high temperature affects the properties of laminate composites, thermo-mechanical modeling is considered.

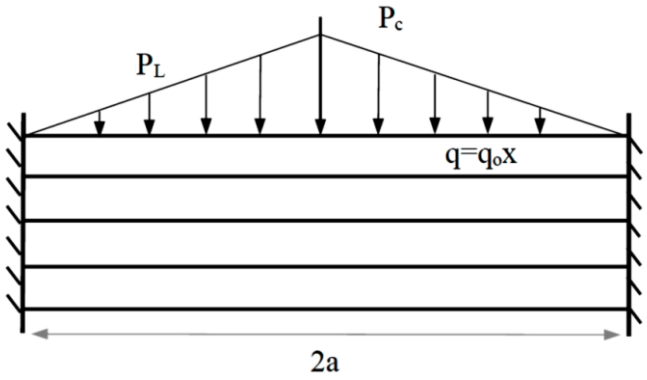

Figure 2-5 Point and linear distributed loads in the delamination zone

2.2 Composite stiffness matrix

Composites as inhomogeneous laminates are different from isotropic materials where each lamina is made of aligned or woven carbon fibers in an epoxy matrix. Every single lamina reinforced with fabric has high stiffness and strength in two perpendicular directions. Equations (1) and (2) illustrate the load-strain equation for a laminate defined by classical plate theory (CPT) [42]. The details of CPT are discussed in Appendix C.

$$\begin{bmatrix} N_x \\ N_y \\ N_{xy} \\ M_x \\ M_y \\ M_{xy} \end{bmatrix} = \begin{bmatrix} [A_{i,j}(x,y)] & [B_{i,j}(x,y)] \\ [B_{i,j}(x,y)] & [D_{i,j}(x,y)] \end{bmatrix} \begin{bmatrix} e_x \\ e_y \\ e_{xy} \\ \kappa_x \\ \kappa_y \\ \kappa_{xy} \end{bmatrix} \quad (1)$$

$$A_{i,j}(x,y), B_{i,j}(x,y), D_{i,j}(x,y) = \int_{-h/2}^{h/2} (1, z, z^2).\bar{Q}_{i,j}(x,y)dz \quad (2)$$

Because of the plane stress assumption, only the elements with i, j = 1, 2, 6 are considered, Equation (3).

$$\begin{bmatrix} N_x \\ N_y \\ N_{xy} \\ M_x \\ M_y \\ M_{xy} \end{bmatrix} = \begin{bmatrix} A_{11} & A_{12} & A_{16}B_{11} & B_{12} & B_{16} \\ A_{12} & A_{22} & A_{26}B_{12} & B_{22} & B_{26} \\ A_{16} & A_{26} & A_{66}B_{16} & B_{26} & B_{66} \\ B_{11} & B_{12} & B_{16}D_{11} & D_{12} & D_{16} \\ B_{12} & B_{22} & B_{26}D_{12} & D_{22} & D_{26} \\ B_{16} & B_{26} & B_{66}D_{16} & D_{26} & D_{66} \end{bmatrix} \begin{bmatrix} e_x \\ e_y \\ e_{xy} \\ \kappa_x \\ \kappa_y \\ \kappa_{xy} \end{bmatrix} \quad (3)$$

2.3 Analytical Modeling

With the help of the plate theory [44], the stress-strain relation is defined in Equation (4), using κ in Equation (4), the radii of curvature.

$$\kappa = \begin{Bmatrix} \kappa_x \\ \kappa_y \\ \kappa_{xy} \end{Bmatrix} = \begin{Bmatrix} -\partial^2\delta/\partial x^2 \\ -\partial^2\delta/\partial y^2 \\ -2\,\partial^2\delta/\partial x\,\partial y \end{Bmatrix} \quad (4)$$

The flexural behavior relates the radii of curvature to the D matrix, (Flexural stiffness), to obtain the unit moments as in Equation (5) :

$$M_{total} = \begin{Bmatrix} M_{xx} \\ M_{yy} \\ M_{xy} \end{Bmatrix} = \begin{bmatrix} D_{11} & D_{12} & D_{16} \\ D_{12} & D_{22} & D_{26} \\ D_{16} & D_{26} & D_{66} \end{bmatrix} \begin{Bmatrix} \kappa_x \\ \kappa_y \\ \kappa_{xy} \end{Bmatrix} - \begin{Bmatrix} M_{xx}^T \\ M_{yy}^T \\ M_{xy}^T \end{Bmatrix} \quad (5)$$

M_{xx} is resultant moment per unit length of y coordinate, M_{yy} is resultant moment per unit length of x coordinate and M_{xy} is the twisting moment caused[31] by

shear stresses perpendicular to the x-axis [45]. In this analysis, only bending due to an out-of-plane load is discussed. M^T, the term expressing thermal moments, is equal to a linear temperature variation times bending stiffness matrix and coefficients of thermal expansion, Equation (6). In symmetric unidirectional composites, since the extension and bending behavior of the laminate are decoupled, therefore the stiffness matrix changes to, Equation (6):

$$\begin{Bmatrix} M_{xx}^T \\ M_{yy}^T \\ M_{xy}^T \end{Bmatrix} = \Delta T\ \kappa^T \begin{bmatrix} D_{11} & D_{12} & 0 \\ D_{12} & D_{22} & 0 \\ 0 & 0 & D_{66} \end{bmatrix} \begin{Bmatrix} \alpha_x \\ \alpha_y \\ 2\alpha_{xy} \end{Bmatrix} \tag{6}$$

α_x and α_y, coefficients of thermal expansion in x and y directions, are defined by the α_1 and α_2, coefficients of thermal expansion in longitudinal and transverse directions (Figure 2-2), of the laminate ply, Equation (7).

$$\alpha = \begin{Bmatrix} \alpha_x \\ \alpha_y \\ 2\alpha_{xy} \end{Bmatrix} = \begin{bmatrix} \cos\phi^2 & \sin\phi^2 & -2\sin\phi\cos\phi \\ \sin\phi^2 & \cos\phi^2 & 2\sin\phi\cos\phi \\ \sin\phi\cos\phi & -\sin\phi\cos\phi & \cos\phi^2 - \sin\phi^2 \end{bmatrix} \times \begin{Bmatrix} \alpha_1 \\ \alpha_2 \\ 0 \end{Bmatrix} \tag{7}$$

Temperature variation is assumed to be linearly through the thickness of the laminate [46] as:

$$\phi(z) = \Delta T z \tag{8}$$

Considering M_{total}, Equation (9), the total amount of the unit moments, the equilibrium equation of a plate will be as in equation (10).

$$M_{total} = [D]\kappa - M^T \tag{9}$$

$$\kappa^T M_{total} = -q \tag{10}$$

where q is the distributed load.

2.3.1 The delamination area

for a unidirectional laminate at any ply, considering the principal directions as parallel and transverse to fibers, a circular area for the layer that the drill bit initially touches can be assumed. Hence the diameter of the circle in the direction of the fibers will grow as the drill bit goes further toward the exit ply. Ultimately the delaminated area at the exit ply is elliptical. Therefore, the ellipticity ratio, η, starts at 1 and grows to larger amounts.

2.3.2 Boundary conditions

In this study, a clamped-clamped boundary condition is assumed. In reality, as studied in the recent papers [47], [48] the boundary condition is between clamped and simply-supported nearly to be clamped.

2.3.3. Crack propagation modes

The first mode of fracture is usually the primary mode for the crack propagation; however, a coupling occurs due to the stress and displacement near the crack area, with different plies orientation. In this case, the release energy rate G_c includes two failure modes. The study in [49] explained that applying the proposed mixed-mode criterion shows a solid prediction of the resultant release energy rate during drilling of CRFP, Equation (11). G_{IC} and G_{IIC} are the energy release rates in the first and second modes of fracture [6, 36].

$$G_C = G_{IC} + (G_{IIC} - G_{IC})\beta^{\zeta} \tag{11}$$

2.3.4. Critical thrust force:

As LEFM (Linear Elastic Fracture Mechanics) explains, tooth movement $d\delta_o$, times the drilling thrust force P equals to work used up in deflecting the plate and propagating the crack, Equation(12).

$$Pd\delta_0 = GdA + dU \tag{12}$$

Equations (13) to (15) define the deflection of an elliptical plate with a and b as dimensions and clamped-clamped boundary conditions under q as a distributed load:

$$\delta_L = (\delta_o)_L(1 - \frac{x^2}{a^2} - \frac{y^2}{b^2})^2 \tag{13}$$

$$(\delta_0)_L = \frac{q = q_0 x}{D_L} \tag{14}$$

According to [50], for an elliptical plate with a clamped edge and bent by linearly varying pressure, the deflection constant D_L is as following:

$$D_L = (\frac{120D_{11}}{a^4} + \frac{32(D_{12} + 2D_{66})}{a^2 b^2} + \frac{24D_{22}}{b^4}) \tag{15}$$

To calculate the deflection of an elliptical plate under point load illustrated in Equations (16) to (18) the same process has been done.

$$\delta_c = (\delta_0)_c(1 - \frac{x^2}{a^2} - \frac{y^2}{b^2})^2 \tag{16}$$

$$(\delta_0)_c = \frac{P_c}{D_c} \tag{17}$$

$$D_c = \pi ab(\frac{6D_{11}}{a^4} + \frac{6(D_{12} + 2D_{66})}{a^2 b^2} + \frac{6D_{22}}{b^4}) \tag{18}$$

Introducing γ, the chisel edge ratio, center point thrust force, and linearly distributed thrust force are as following:

$$P_c = \gamma P_{total} \tag{19}$$

$$P_L = (1 - \gamma)P_{total} \tag{20}$$

The same notation order will help to calculate the total virtual work of the external loads as follows:

$$W_{total} = W_c + W_L \tag{21}$$

Equations (22) and (23) represent [41], the virtual work done by the external loads corresponding to the work of (q_L), and (q_c).

$$W_L = \int_{-a}^{a} \int_{-b\sqrt{1-\frac{x^2}{a^2}}}^{b\sqrt{1-\frac{x^2}{a^2}}} \delta_L q_L dxdy \tag{22}$$

$$W_c = \int_{-a}^{a} \int_{-b\sqrt{1-\frac{x^2}{a^2}}}^{b\sqrt{1-\frac{x^2}{a^2}}} \delta_c q_c dxdy \tag{23}$$

As $q_L = q_o x$, the linear distributed load, and $q_c = P_c/\pi ab$, concentrated load. Also, the distributed portion of the thrust force (P_L), has a constant named, linearly distributed load constant, that is shown with q_o and is expressed as follows:

$$P_L = \int_0^a \pi(ax + b)(q_o x)dx \tag{24}$$

Therefore,

$$q_o = \frac{P_L}{\pi(\frac{a^3}{2} + \frac{ba^2}{2})} \tag{25}$$

Defined strain components as following, Equation (26), is included in the strain energy of the delaminated area, Equation (27).

$$\varepsilon = \begin{Bmatrix} \varepsilon_x \\ \varepsilon_y \\ \varepsilon_{xy} \end{Bmatrix} = z \begin{Bmatrix} \kappa_x \\ \kappa_y \\ \kappa_{xy} \end{Bmatrix} - z \begin{Bmatrix} \alpha_x \\ \alpha_y \\ 2\alpha_{xy} \end{Bmatrix} \Delta T \tag{26}$$

$$U = \frac{1}{2}\int < \varepsilon, \sigma > dV = \frac{1}{2}\int \varepsilon^T \sigma dV \tag{27}$$

Referring to Equation(26), Equation (27) will be also written as follows:

$$U = \frac{1}{2}\int [z\kappa - z\alpha\Delta T]^T [Q][z\kappa - z\alpha\Delta T]dV \tag{28}$$

$$D_{ij} = \sum_{k=1}^{n} (\bar{Q}_{ij})(\frac{z_k^3 - z_{k-1}^3}{3}) \tag{29}$$

Considering Q_{ij} the bending stiffness terms and using the theory of laminates and the bending stiffness matrix, D_{ij}, calculated in Equation (30), and taking the integral

term over the laminate thickness, the strain energy of the delaminated area is as the following:

$$U = \frac{1}{2}\int [\kappa - \alpha\Delta T]^T [D][\kappa - \alpha\Delta T]\, dS \tag{30}$$

By incorporating Equation (9),

$$U = \frac{1}{2}\int \int [\kappa - \alpha\Delta T]^T M_{total}\, dxdy \tag{31}$$

As shown in Figure 2-5, the total strain energy of the area is the sum of the strain energy due to linearly distributed load and the strain energy due to center point load, Equation (32). For further calculation of the strain energies, δ_L and δ_c, according to Equations (13) and (16) are included as the deflections of the area, respectively.

$$U_{total} = U_c + U_L \tag{32}$$

$$U_L = \frac{1}{2}\int_{-a}^{a}\int_{-b\sqrt{1-\frac{x^2}{a^2}}}^{b\sqrt{1-\frac{x^2}{a^2}}} [\kappa(\delta = \delta_L) - \alpha\Delta T]^T M_{total} \quad dxdy \tag{33}$$

$$U_c = \frac{1}{2}\int_{-a}^{a}\int_{-b\sqrt{1-\frac{x^2}{a^2}}}^{b\sqrt{1-\frac{x^2}{a^2}}} [\kappa(\delta = \delta_c) - \alpha\Delta T]^T M_{total} \quad dxdy \tag{34}$$

Delamination energy, U_d, is derived by multiplying the total critical energy release rate, G_C, by the damaged area surface.

$$U_d = G_C \pi ab \tag{35}$$

To determine the critical thrust force, the theory of virtual work is implemented in the delaminated part of the plate affected by drilling. In this case, the induced work from the external forces is equal to the potential energy variation added by the energy absorbed by the peeled parts of the plate,

Considering the theory of virtual work, the amount of work done by the external forces is equal to the energy dissipated by delamination and energy absorbed by the peeled parts of the plate,

$$\partial W = \partial U + \partial U_d \tag{36}$$

The delamination area increasing rate is given by:

$$\partial A = \pi(a + \partial a)(b + \partial b) - \pi ab = \pi(a.\partial b + b.\partial a) = 2\pi b.\partial a \tag{37}$$

Therefore,

$$\partial U_d = 2G_C \pi b\, \partial a \tag{38}$$

With previous calculations and assumptions, Equation (39) predicts the critical thrust force. In Appendix A, more details about the constants in the thrust force equation can be found.

$$P = 12 D_c D_L a^4 b^3 \left(\frac{b\gamma D_L - D_I}{D_{II}}\right) \tag{39}$$

Ellipticity ratio and chisel edge ratio are decided after selecting the material of the workpiece and the diameter of the drill bit. With determined composite plate stiffness matrix and plate deflection, the critical thrust force is estimated by strain energy methods.

2.4 Verification and Discussion

In this section, the proposed analytical model is investigated with three different sets of experimental results obtained from the open literature. A thorough summary of previous analytical models, the chosen delamination area, and the predicted thrust force have been discussed in Table 1-1. Hence, the new model takes into consideration the thermo-stresses caused by drilling, the mixed mode of fracture, and also growing η, the ellipticity ratio, from the circular area on the entrance layer to the elliptical area on the exit layer. The thrust force is predicted to be the mixture of a center point load and a linearly distributed load.

The plots of critical thrust force versus the number of laminated plots, have an x-axis starting layer number four (entrance layer) to layer number one of the composite (the exit layer).

To compare the accuracy of the new analytical model with the experimental data, the Average Accuracy Model (AAM) is utilized. In this model, the accuracy of the critical thrust force in each layer is initially calculated and then the average of the accuracy for all four layers is reported.

Average Accuracy is the average of each accuracy per level (total of the accuracy for each level estimated/number of levels).

$$AAM = \frac{\sum_0^n \left[1 - \left[\frac{ABS[Analytical\ result - Experimental\ result]}{Experimental\ result}\right]\right]}{n} \quad (40)$$

2.4.1 Case study 1

For the Lachaud-Piquet model [51], test plates, manufactured by one-directional 914/T300 CFRP, have 24 plies in quasi-isotropic lay-up. All the modes of rupture damages are done principally by delamination. A previous study calculated values of critical energy release rates [52] by the compliance method. al properties of the workpiece.

Table 2-1 includes the mechanical properties of the workpiece.

Table 2-1 Mechanical Properties, Piquet and Lachaud [52]

Composite Material	E_1 (GPa)	E_2 (GPa)	G_{12} (GPa)	ν_{12}	v_f	Ply Thickness (mm)	Ply Orientation
914/T300 CFRP	144	8.7	4.14	0.3	0.59	0.125	Quasi-Isotropic

Quasi-isotropic laminates perform close to isotropic materials at the laminate level while their plies might be orthotropic or anisotropic according to the main coordinates.

The strength properties, however, will vary with direction. Five different analytical models, as Piquet[52], Lachaud[52], Jain[33], Girot[36], Ismail[46] besides the new proposed model are compared to the experimental data (i.e., Exp) in Figure 2-6.al properties of the workpiece.

Table 2-1 contains a calculated average accuracy model (AAM) of each one. Furthermore, the total result improvement with variable η and β is concluded. The new model has an average accuracy model of 81.90%.

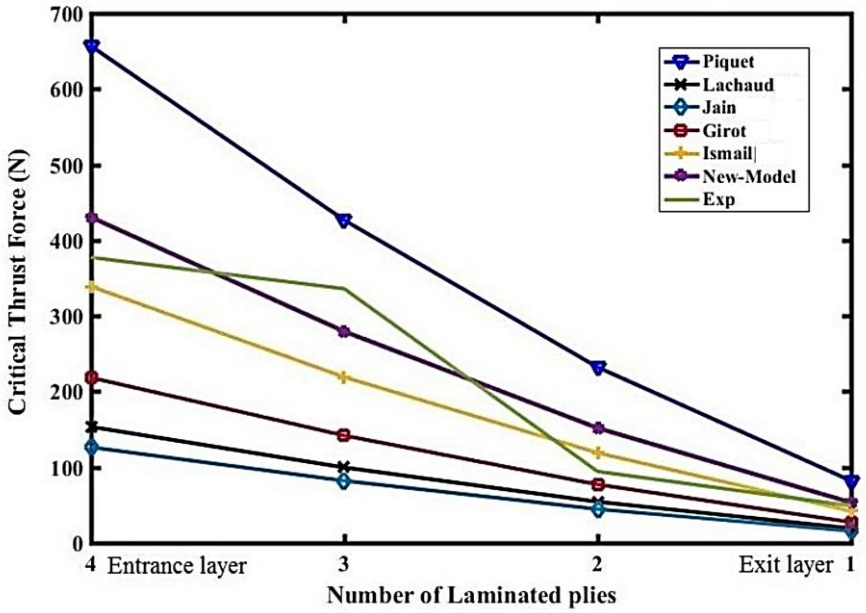

Figure 2-6 Analytical and experimental results, Drill diameter=4.8 (mm), cutting speed=51 (mm/min), layer 4 is the entrance number, and layer 1is the exit

Table 2-2 Thrust Force (N) Average Accuracy Comparison of each Analytical Model in the open iterature , Piquet-Lachaud example [52]

Source of data	Number of layers 1	2	3	4	AAM (%)
Piquet	26.42	56.6	94.34	154.72	45.74
Lachaud	86.79	222.64	426.42	633.96	23.03
Jain	15.79	44.67	82.07	126.36	36.48
Girot	27.305	77.23	141.88	218.44	63.05
Ismail	37.73	106.81	196.71	304.30	76.75
New Model	44.02	123.68	226.83	348.98	81.90
Experiments	49.05	94.33	335.84	377.35	

2.4.2 Case study 2

For the next set of experiments, Ismail [46] had chosen the following composite with mechanical properties written in Table 2-3. In this comparison, the new model average accuracy is 84.02%. Ismail model also takes benefits from thermo-mechanical modeling and the elliptical delamination area with a combined center point and uniformly distributed load.

Table 2-3 Mechanical Properties, Ismail[46]

Composite Material	E_1 (GPa)	E_2 (GPa)	G_{12} (GPa)	ν_{12}	v_f	Ply Thickness (mm)	Ply Orientation
CFRP	175.9	8.1	4.4	0.32	0.6	0.3125	Cross-Ply

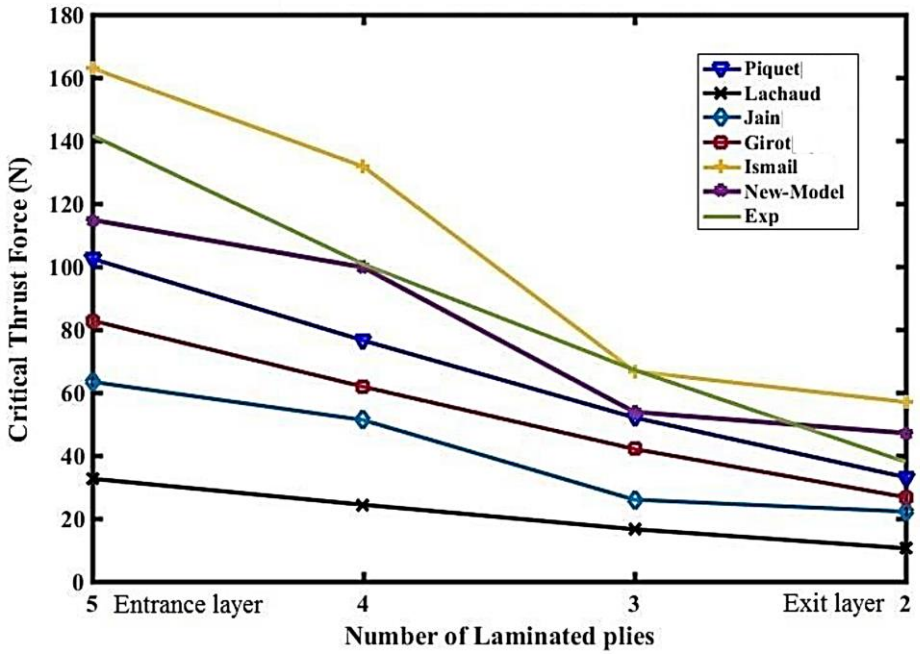

Figure 2-7 Analytical and experimental results, Drill diameter= 6 mm, Feed rate=0.18mm/rev layer 4 is the entrance number and layer 1is the exit

Table 2-4 Thrust Force (N) Average Accuracy Comparison of each Analytical Model in the literature review, Ismail example [46]

Source of data	Number of layers 2	3	4	5	AAM (%)
Piquet	22.55	41.43	63.78	89.14	78.23
Lachaud	7.17	13.18	20.29	28.36	24.89
Jain	15.10	20.65	42.72	55.12	48.15
Girot	18.22	33.48	51.54	72.04	63.22
Ismail	38.84	53.11	109.86	141.76	75.85
New Model	33.61	42.06	94.54	104.96	84.02
Experiments	37.95	67.15	100.73	141.60	

2.4.3 Case study 3

The last set of experiments is reported in Girot [36]. Table 2-5 has the mechanical properties for the T800/923C CFRP chosen for the experiment. The Girot analytical model benefits from linearly distributed load plus a center point load and also mixed-mode of fracture in a circular delamination area.

Table 2-5 Mechanical Properties, Girot [36]

Composite Material	E_1 (GPa)	E_2 (GPa)	G_{12} (GPa)	ν_{12}	v_f	Ply Thickness (mm)	Ply Orientation
T800/923C CFRP	150.31	7.58	3.93	0.35	0.59	0.182	[45 45 0 45]

Result improvement in this section is more significant than the last two sets. The average accuracy model is 90.69%. The chosen chisel edge ratio, γ, in these three analytical comparisons is between 0.3 and 0.7. The variable ellipticity ratio, η, starts from 1 for the entrance layer and ends at 1.25 for the exit layer.

In terms of the analysis of the results, the new model is successful to predict a more accurate drilling thrust force with help of the mixed-mode of fracture analysis and variable ellipticity ratio.

In detail, considering mixed-mode of fracture contributes more to the new model rather than the variable ellipticity ratio.

Depending on the type of the composite and ply orientation the range of the resulting improvement differs from 2.80% to 26%.

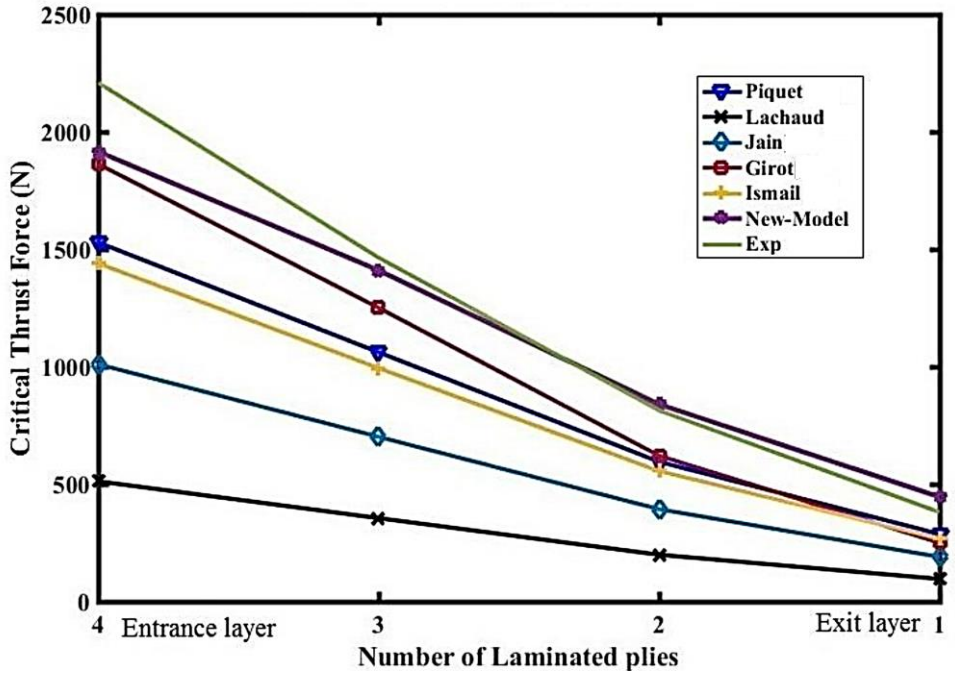

Figure 2-8 Analytical and experimental results, Drill diameter= 10.8 mm, Feed rate=45m/min layer 4 is the entrance number and layer 1is the exit

This study focused on four substantial points to predict the critical thrust force,

(i) Unidirectional composite structures are exposed to both modes I and II, therefore a proportionate critical energy release rate is required,

(ii) Since high temperature affects properties of laminate composites, thermo-mechanical modeling is considered

(iii) The delamination area starts as a circular area and grows into an elliptical area in the same direction as the fibers,

(iv) Part of the thrust force is a center point load, modeling the chisel edge force, and the other part of it is a linearly distributed load, modeling the cutting lip force.

Table 2-6 Thrust Force (N) Average Accuracy Comparison of each Analytical Model in the literature review, Girot example [36]

Source of data	Number of layers 1	2	3	4	AAM (%)
Piquet	142.65	595.09	741.24	1141.22	72.57
Lachaud	47.73	199.13	248.03	381.87	24.28
Jain	94.25	393.18	489.74	754.01	47.95
Girot	250.65	620.81	1250.73	1863.21	77.97
Ismail	133.15	555.87	696.45	1082.13	67.94
New Model	221.59	923.13	1149.74	1769.92	90.69
Experiments	380.54	813.95	1464.06	2209.30	

After demonstrating the mathematical modeling, the new analytical model for the thrust force is compared with five different analytical models from the literature review in three different sets of experiments. Overall, the new analytical model improves the results by 2.80% in the first, 11.35% in the second, and 26.38 % in the last set of experiments. Further improvement of this delamination model to multi-directional laminates with feed rate analysis and a new set of experiment accompanying will be discussed in future work.

Chapter 3. Numerical Modelling for drilling Composites

Carbon fiber reinforced polymers (CFRP) withstand fatigue excellently, which makes them materials of choice in the aerospace industry. High strength to weight ratio and high stiffness are only a few of their phenomenal characteristics.

Since the introduction of CFRPs a few decades ago, there has been a significant increase in their application. The replacement of conventional aluminum material by CFRPs in Airbus A350XWB aircraft has been reported to be about 50% on its structural weight [53].

Composite manufacturing includes two categories, primary or secondary [54]. CFRPs are mainly manufactured via the primary manufacturing processes and additional machining processes are needed, such as drilling, to assist the assembly [55]. Drilling with a standard twist drill is currently the most common method of hole making, for rivets and bolts, included in the assembly. Despite their interesting nature, composites can complicate the drilling process in comparison to metals [56].

Numerical simulation of machining processes has been more common in recent years with help of advanced computers. This research discusses the suitable material properties, failure criteria, workpiece, and drill bit geometry characteristics for an accurate simulation of the delamination. The core purpose is to study the effect of a drill bit geometric parameters such as chisel edge width, helix angle and point angle on delamination.

The number of numerical research utilizing finite element method (FEM) have been ascending because of the computational power improvements and new simulation methods.

They are many discussions in this field about analyzing the drilling process in 2D or 3D. Validation of 2D approaches to fiber reinforced composite drilling has been discussed in [13,14]. Out-of-plane failure in orthogonal cutting of composites using a 3D FE model illustrates more accurate simulations. Taking into account the effect of stacking sequence on the damage propagation, the delamination has to be simulated with cohesive zone interactions.

Finite element analysis in drilling numerical models was designed to define inter-laminar damage in composites [12]. In numerical modelling, once the model is verified to be functional, it could be a useful tool to determine the parameters affecting the drilling process and providing accurate prediction to examine these parameters [13].

Numerical analysis is capable of minimizing the experimental expenses and therefore enhancing the efficiency [57]. As a result, the finite element method (FEM) is valuable in modeling and examining the damage of composite in different machining parameters. Material removal modeling in orthogonal cutting and carbon fiber reinforced fracture were studied using FEM by Van Luttervelt et al. [58] and Mahdi et al. [59]. In this study, the goal is to examine ply orientations to evaluate the delamination effect upon drilling and visualize the growth of delaminated area in a complete 3D model simulation.

3.1 Intra-laminar damage

The study of UD-CFRP failure criteria assessment was studied starting 1998 to 2004. During this time a group of researchers participated in a study, gathering all the best available composite failure models. Each failure model was associated with a wide set of experimental outcomes. The qualities and flaws of the individual model were clear, and suggestions were applied to improve the failure models.

3.2 Hashin Criteria

The Hashin criteria are an alteration to the Hashin-Rotem criteria to consider the matrix strength with the beneficiary effect of compressive stresses [60]. Agreeing with Hashin, the plane stress tensile fiber failure criterion is now:

$$\left(\frac{\sigma_{11}}{S_{11,T}}\right)^2 + \left(\frac{\tau_{11}}{S_{12}}\right)^2 \geq 1 \tag{41}$$

And the compressive fiber failure is as:

$$\left(\frac{\sigma_{11}}{S_{11,C}}\right)^2 \geq 1 \tag{42}$$

For tensile matrix failure:

$$\left(\frac{\sigma_{22}}{S_{22,T}}\right)^2 + \left(\frac{\tau_{12}}{S_{12}}\right)^2 \geq 1 \tag{43}$$

And compressive matrix failure:

$$\left(\frac{\sigma_{22}}{2\,S_{23}}\right)^2 + \left[\left(\frac{S_{22,C}}{2\,S_{23}}\right)^2 - 1\right]\frac{\sigma_{22}}{S_{22,C}} + \left(\frac{\tau_{12}}{S_{12}}\right)^2 \geq 1 \tag{44}$$

3.3 Puck criteria

The Puck [61] theory includes five distinct specific failure criteria. These are fiber tensile failure, fiber compressive failure and three failure modes in shear as in shear and tensile failure, predominantly shear failure, and finally shear and compression failure. Tensile fiber failure:

$$\left(\frac{\sigma_{11}}{S_{11,T}}\right)^2 \geq 1 \tag{45}$$

Compressive fiber failure:

$$\left(\frac{\sigma_{11}}{S_{11,C}}\right)^2 \geq 1 \tag{46}$$

Tensile matrix failure occurs when:

$$\sqrt{\left(\frac{\tau_{12}}{S_{12}}\right)^2 + \left(1 - p_{12}^{+}\frac{S_{22,T}}{S_{12}}\right)^2 \left(\frac{\sigma_{22}}{S_{22,T}}\right)^2} + p_{12}^{+}\frac{\sigma_{22}}{S_{12}} \geq 1 \tag{47}$$

Compressive matrix failure:

$$\frac{1}{S_{12}}\sqrt{\tau_{12}^2 (p_{12}^{-}\sigma_{22})^2} + p_{12}^{-}\sigma_{22} \geq 1 \tag{48}$$

And,

$$\left[\left(\frac{\tau_{12}}{2(1+p_{22}^{-})S_{12}}\right)^2 + \left(\frac{\sigma_{22}}{S_{22,C}}\right)^2\right]\frac{S_{12}}{-\sigma_{22}} \geq 1 \tag{49}$$

Where $p_{12}^{-}, p_{12}^{+} and\ p_{22}^{+}$ are the Puck inclination parameters, formulated in Puck (2002). Puck criteria are three dimensional.

3.4 Inter-laminar damage

In recent publications, delamination is the focal topic of research in CFRP composites machining. It is discussed as the most serious defect because it decreases the strength of the structure and composite reliability part in the structure lifecycle.

3.4.1 Cohesive zone elements

Researchers [55], [25] have applied this Inter-laminar failure model for delamination defect in composites simulations. Therefore, cohesive elements presented in Abaqus/CAE, with 5 micrometers in thickness are utilized in the layer interfaces. The mechanical properties of this interface are calculated in Equation below [62].

$$K = \frac{\alpha E_{33}}{t} \tag{50}$$

Where K interface stiffness, E_{33} Young's modulus of CFRP laminate, t ply thickness, and α is an adjustable parameter.

For α greater than 50, the stiffness decrease is less than 2% due to the presence of the interface [55]. Cohesive elements damage initiation can be formulated [62, 63]as in Equation (51) below.

$$\left[\frac{t_n}{t_n^0}\right]^2 + \left[\frac{t_s}{t_s^0}\right]^2 + \left[\frac{t_t}{t_t^0}\right]^2 = 1 \tag{51}$$

Where t_n , t_s, and t_t are the instantaneous values of normal and shear tractions, however t_n^0 , t_s^0, and t_t^0 characterize the highest values of nominal stress. As soon as the damage initiation condition is satisfied, delamination prompts and stiffness starts to decrease linearly compared to damage variable, similar to cohesive layer. The material properties to model cohesive elements in interface layer can be found in Table 3-1.

Table 3-1 material properties for the cohesive layer

Parameter	Value
t_n^0 (MPa)	60
$t_s^0 = t_t^0$ (MPa)	90
G_n (N/mm)	0.2
$G_s = G_t$ (N/mm)	1
K_n (N/mm^2)	4×10^6
$K_s = K_t$ (N/mm^2)	4×10^6

3.5 Vectorized user-defined material to model the failure criteria in Abaqus/Explicit

The Abaqus/CAE software should be operating with Intel Fortran composer and Microsoft Visual studio.

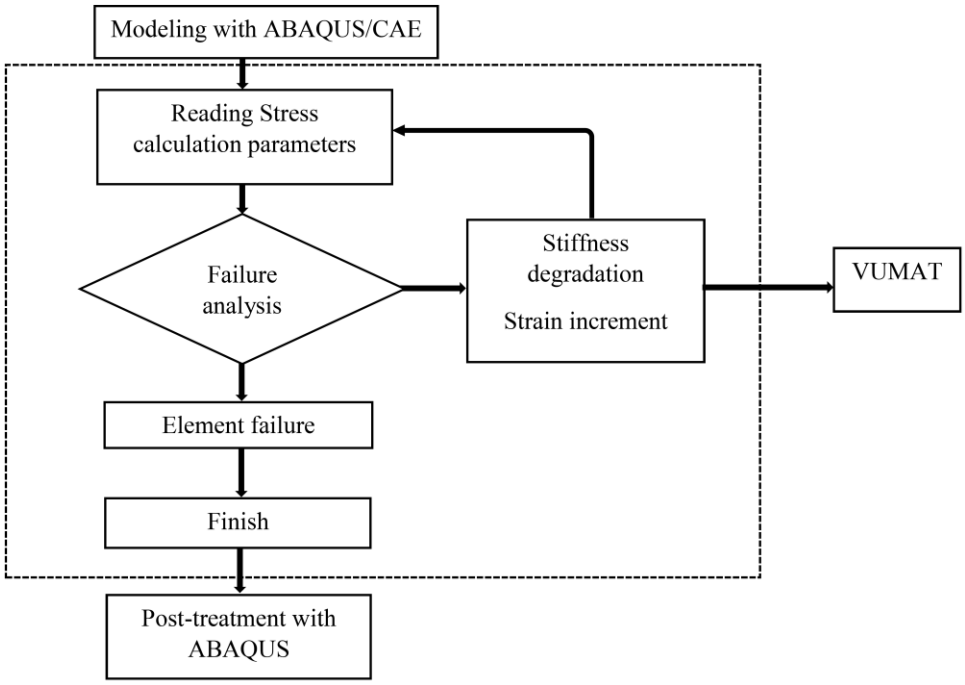

Figure 3-1 Vectorized user-defined material to model the failure criteria in Abaqus/Explicit [55]

The VUMAT model is programmed in Fortran compiler and browsed for the job analysis of the Abaqus/CAE. Figure 3-1 illustrates a simple execution of the failure criterion in Abaqus/Explicit.

3.6 Modeling steps

The process considered in a FE model in Abaqus/CAE are illustrated as a process flow in Figure 3-2.

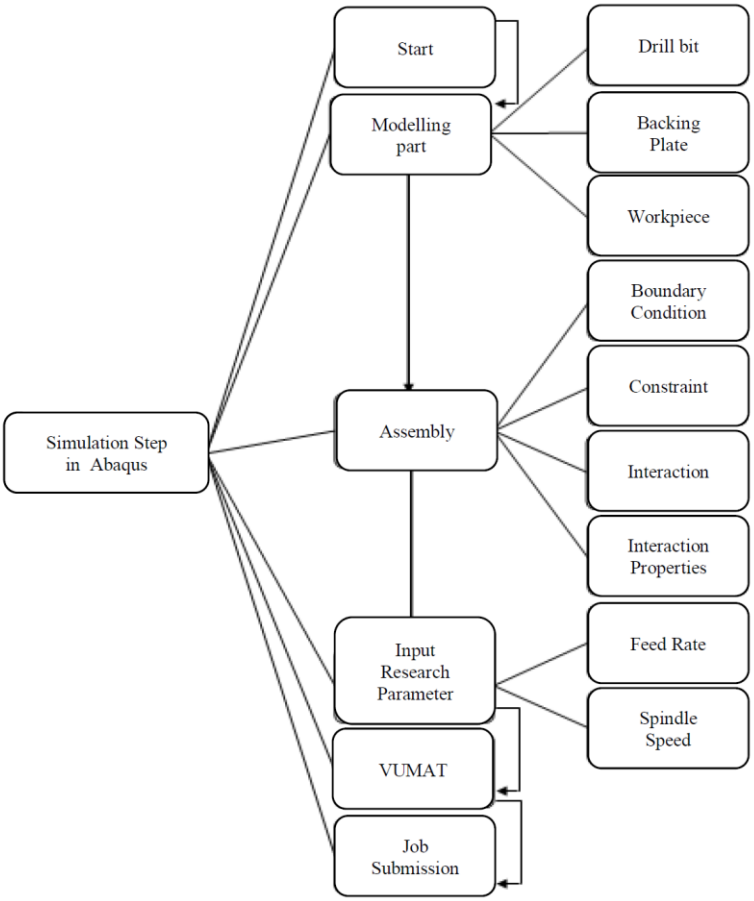

Figure 3-2 Process Flow (ABAQUS, Dassault Systemes ®)

3.7 Part modeling

The unidirectional composite plate and the drill bit are designed as 3D Solid and Deformable. The drill bit is modeled SOLIDWORKS and imported to Abaqus/CAE.

3.8 Property selection

The plate material Properties are considered as mechanical constants in VUMAT subroutine for 3D failure criteria implementation. The tool and the composite plate are both modeled as solid homogenous sections and given in this module. Ultimately, material orientation based on the ply orientation is considered. The most commonly ply orientations designed as (0°, -45°, 90°, 45°) lay-up.

3.9 Assembling

The assembly of the whole simulation set up can be seen in Figure 3-3

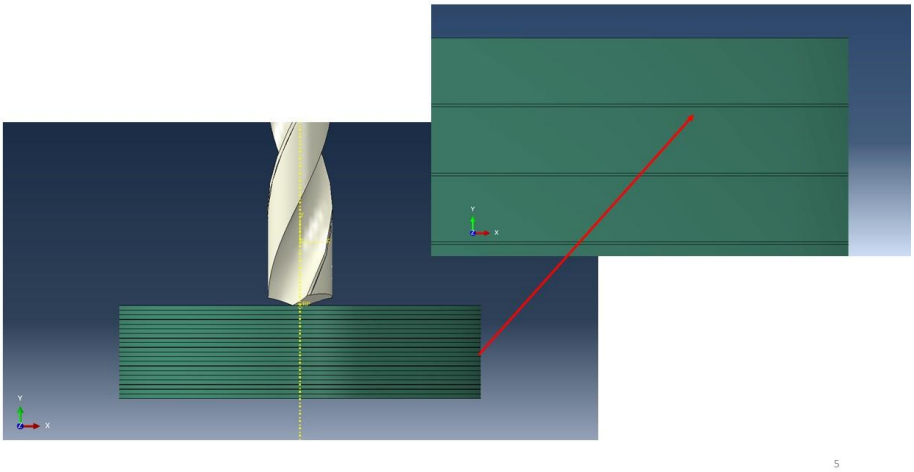

Figure 3-3 Simulation set up with cohesive zone elements

3.10 Meshing

Meshes are generated on parts formed in Abaqus/CAE. Different approaches of mesh control are offered within the requirements of the analysis. There are three different common mesh designs in Abaqus Eulerian, Lagrangian, and Arbitrary Lagrangian-Eulerian [22]. The table below illustrates the differences among these methods.

The common elements for unidirectional carbon fiber reinforced composites are Eight-node brick element with reduced-Integrated (C3D8R) and, COH3D8 type elements for cohesive zone elements are utilized in the simulation. For more accurate results the mesh in the damaged area around drilled hole is finer closely to three times. The solution convergence is partially decided by the size of the element. It is common to have convergence considering an alignment between the element size and the convergence without decreasing the accuracy of the simulation [63].

While the drill bit includes the same element size as the plate, the elements are selected rigid with respect to a reference point, usually the tip of the drill bit. A rigid body including elements sets with the displacement directed in respect to a reference node. The relative distances between the nodes of the rigid body remain constant and non-deforming throughout the entire simulation.

Table 3-2 Meshing methods [63]

Mesh type	Specifications	Appropriate for machining
Eulerian	Spatially fixed Material flowing allowance through the volume	No
Lagrangian	Attached mesh to the material Deforms similarly to actual machining Severe distortion The constant need for re-meshing	Yes Higher computational cost
Arbitrary Lagrangian-Eulerian (ALE)	Combines the advantages of Eulerian and Lagrangian Avoids severe distortion	Yes

3.11 Mesh sensitivity

Mesh size selection is one of the most crucial elements in FEA. There is a fine line here; coarser elements increases the possible error in the simulation, while finer elements increase computing time. There is a balance between computing time and accuracy. In some instances, computing time can increase twice to improve accuracy

by only 1%. In the table below, the thrust force results for each mesh size is verified by the thrust force introduced in analytical model discussed and verified in the previous chapter.

Table 3-3 Effect of mesh size of thrust force error for a feed rate of 300 (mm/min)

Thrust Force in the exit layer, Analytical (N)	Mesh size (μm)	Thrust Force, Numerical (N)	Error (%)
185.7	50	213.555	15
	45	206.127	11
	40	200.556	8
	35	198.327	6.8
	30	196.099	5.6
	25	193.499	4.2
	20	192.571	3.7
	15	192.385	3.6
	10	191.8281	3.3
	5	191.271	3

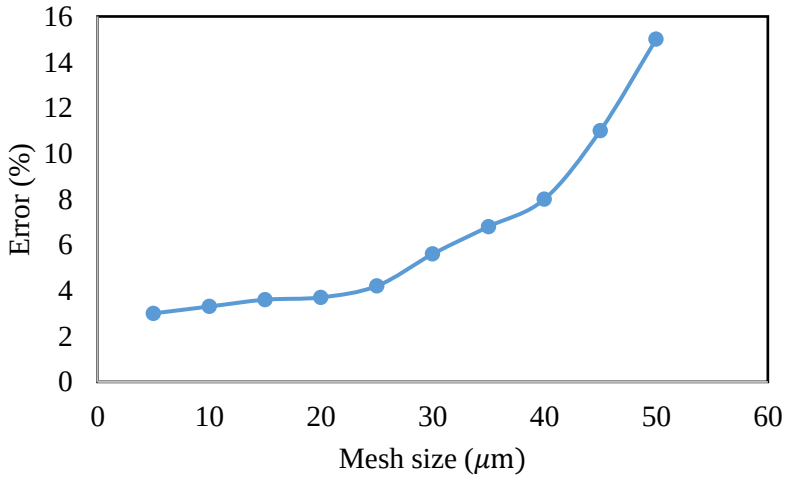

Figure 3-4 Thrust force error vs. mesh size

3.12 Interaction module

Interaction properties control the way the drill bit and the plate are about to interact throughout the composite drilling procedure. The interactions between the layers are introduced separately from the contact between the tool and workpiece. Generally, the interaction between the drill bit and the workpiece is penalty type with friction coefficient 0f 0.3. Cohesive zone elements are determined between every two layers of the laminates, with parameters determining initiation, evolution, and stabilization [63].

3.13 Boundary conditions

All the boundary conditions for the drill bits are given to the drill bit's reference point. With incorporating the velocity boundary condition, the feed rate and the spindle speed are given to the reference point in z-direction. CFRP composite plates are simulated as clamped with vertical edges fixed. Figure 3-5 illustrates the setup.

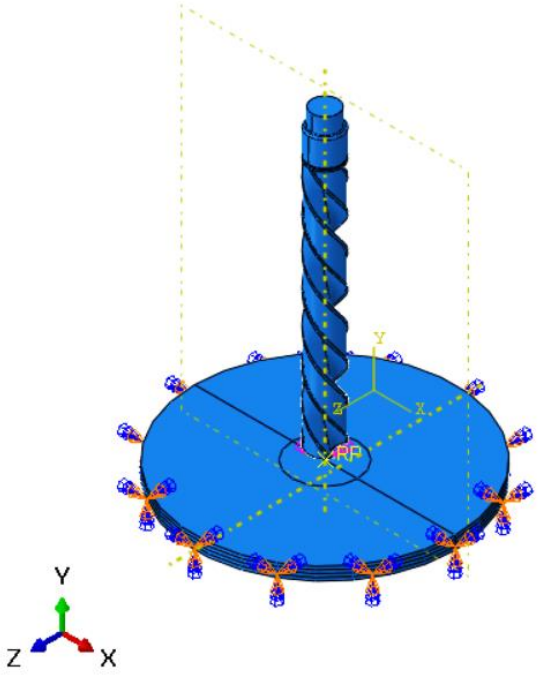

Figure 3-5 Model assembly

3.14 Model validation

In [55] the following material was used for running experiments and simulation.

Table 3-4 Verification model mechanical properties

E_{11}	$E_{22} = E_{33}$	$\upsilon_{12} = \upsilon_{13}$	υ_{23}	$G_{12} = G_{13}$	G_{23}	ρ
127 GPa	9.1 GPa	0.31	0.45	5.6 GPa	4 GPa	1600 kg/m^3

The results of the current simulation verified with the experimental and numerical results published in [55].

Table 3-5 Verification results

Feed rate	Thrust Force (N)		
(mm/min)	Experiments Results [55]	Current simulation	AAM (%)
150	115	127.4	89
300	170	185.7	91.2
500	200	215.9	92

3.15 Visualization of delaminated area progress from circular to elliptical

Simulation results for a 4 layer unidirectional carbon fiber reinforced composite. The results of the unidirectional composite, the damaged area geometry agree with the analytical predictions. In this FE simulation, the lay-up of the composite is [0, +45, 90, -45], Figure 3-8.

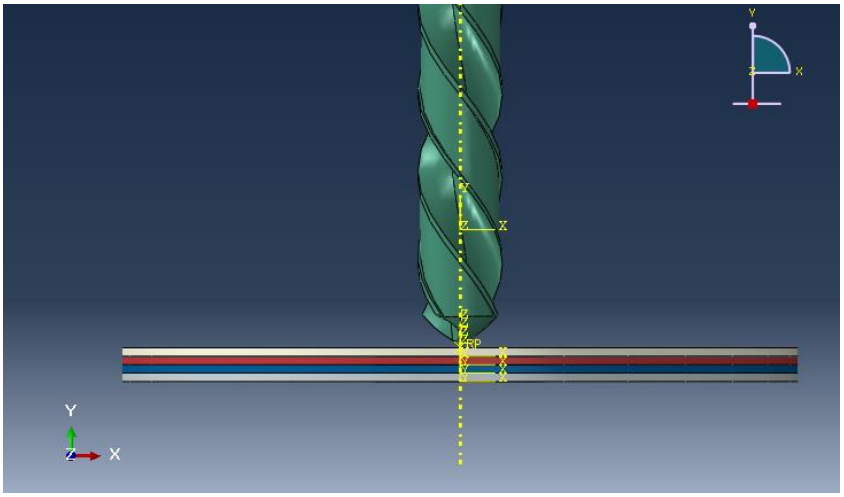

Figure 3-6 Simulation set up

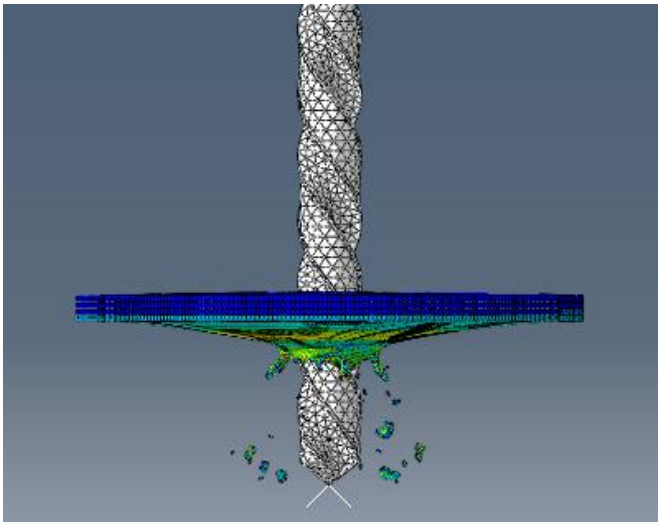

Figure 3-7 Simulation process

3.16 Measuring Delamination

One of the methods of measuring delamination damage is delamination factor (F_d), defined as the one-directional proportion of the maximum diameter (D_{max}) of the damaged zone to the nominal diameter (D_{nom}), Equation 52.

$$F_d = \frac{D_{max}}{D} \tag{53}$$

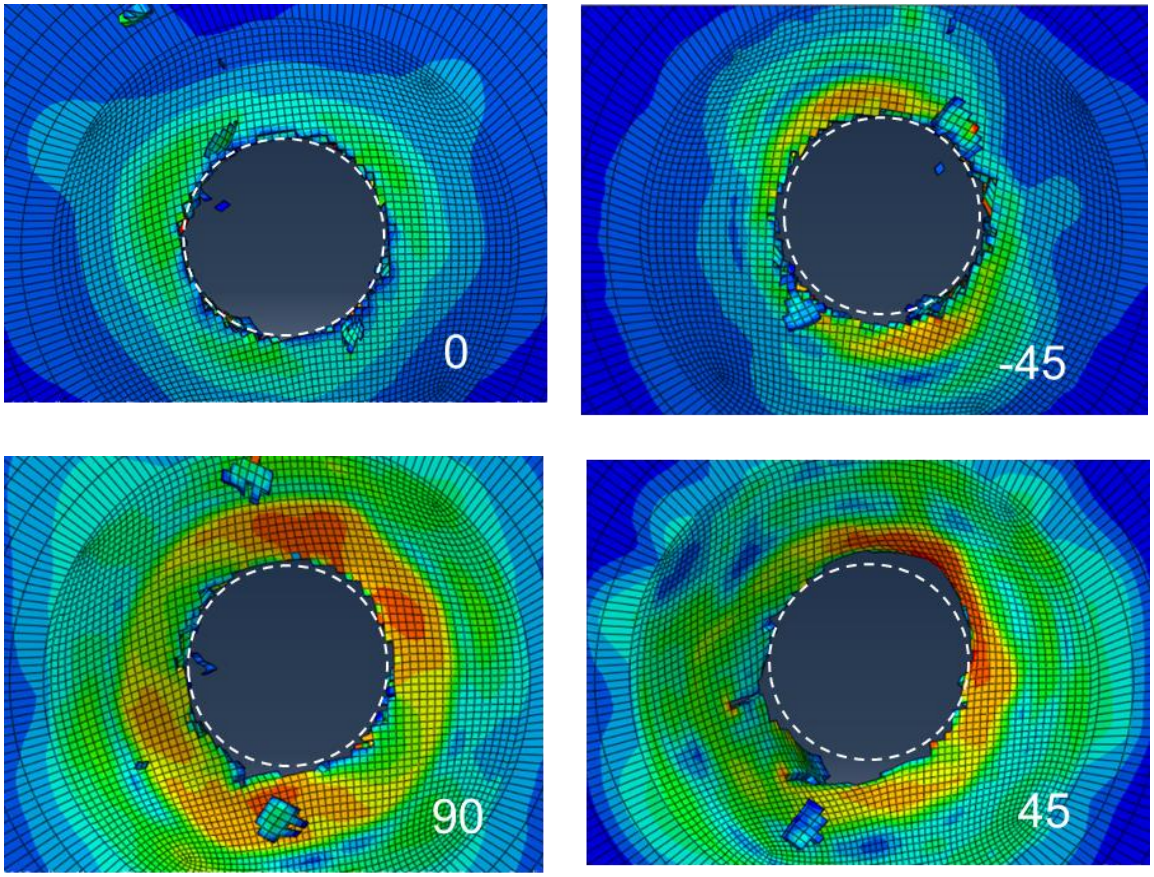

Figure 3-8 Entrance to exit (left to right) delaminated area with lay-up [0, -45, 90, and 45]

Figure 3-9 shows the way to assess (D_{max}) and (D_{nom}) in a drilled damaged area. A number of researchers proposed a 2D delamination factor F_a as formulated in Eq. (54) where A_{nom} and A_{del} can be introduced as nominal and delaminated areas as illustrated in Figure 3-9.

$$F_a = \left(\frac{A_{del} - A_{nom}}{A_{nom}}\right)\% \tag{54}$$

Most researchers have quantified the intensity of delamination incorporating the delamination factor which is the ratio between the most extreme delaminated area and the nominal area. The finite element software utilized color spectrum to demonstrate the intensity of the damaged area.

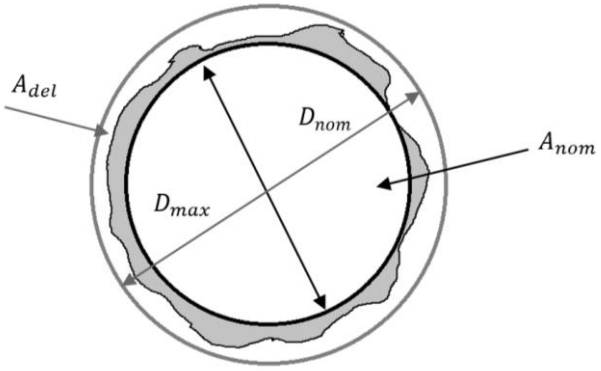

Figure 3-9 Delamination areas

3.17 Tool geometry

A table for presenting the features of the drills, in 8 mm diameter.

Table 3-6 Drill bits geometry specifics

Chisel edge width (mm)	1.19	1.90	2.61	3.31
Point angle (degrees)	135			
Helix angle (degree	27			

At this point, the focus is on the chisel edge width effects on the thrust force. Four different drill bit designs will be used in the simulation to investigate this matter.

3.17.1 Chisel edge width

The chisel edge (Figure 3-10) is situated in the center of the drill tip and has no role in cutting the material. The chisel edge penetrates the material and displaces the material with indentation mechanism.

These undesired parameters for the drilling process increasing heat generation and power consumption.

Figure 3-10 Chisel edge

In another study [33] of the impact of chisel edge was discussed with drilling holes in various chisel edges and maintaining point angles and machining parameters unaltered with 1/4 in in diameter drill bit.

The chisel edge massively affects the thrust force and delamination factors. Based on these simulations, it turned out to be obvious that the main contributor to the thrust force is the chisel edge and therefore the existence of delamination in the exit ply.

The area delamination factor here starts at 1.025 and increases to 1.08, 1.11, and 1.12 with the increase of the chisel edge width. In a previous attempt [33] for ¼ inch drill, a set of experiments was executed. The profile of thrust force changes here agrees with the experiments in [33].

It is illustrated here that a linear profile is happening between the increase of the thrust force and the increase of the chisel edge width.

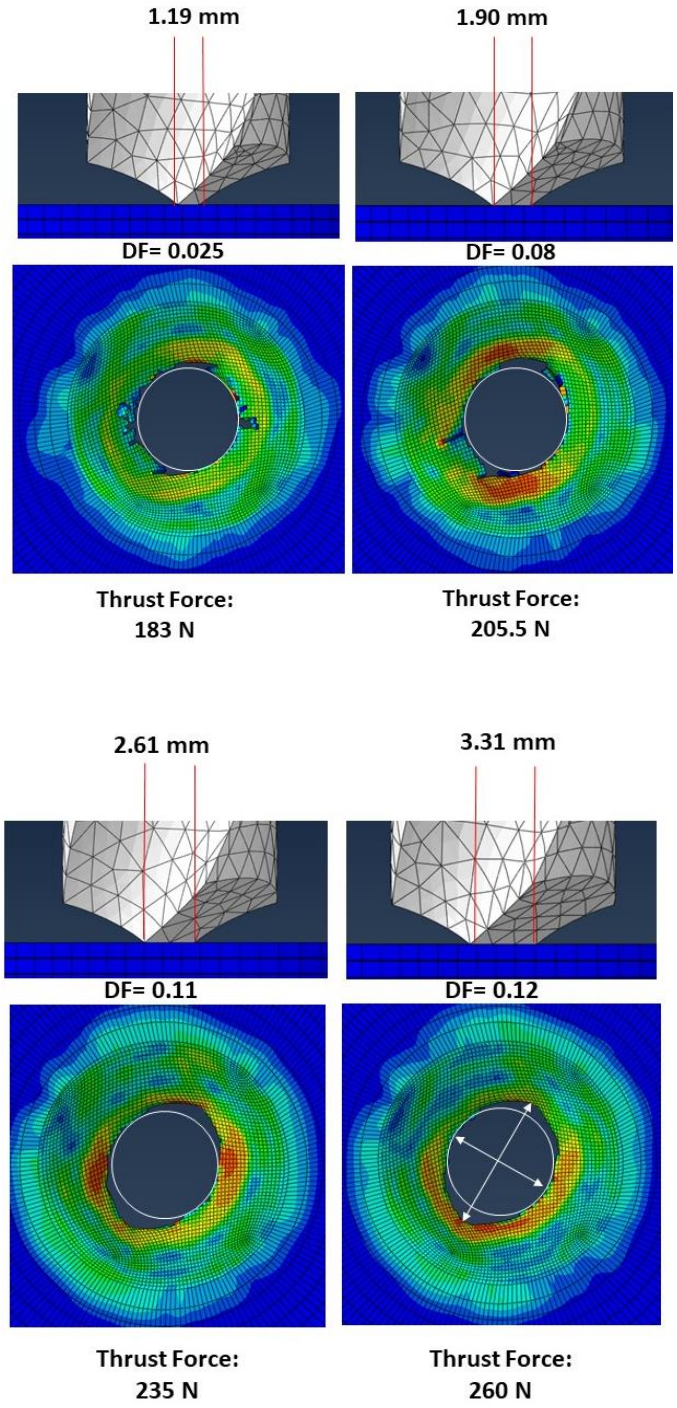

Figure 3-11 Effect of chisel edge on the delaminated area

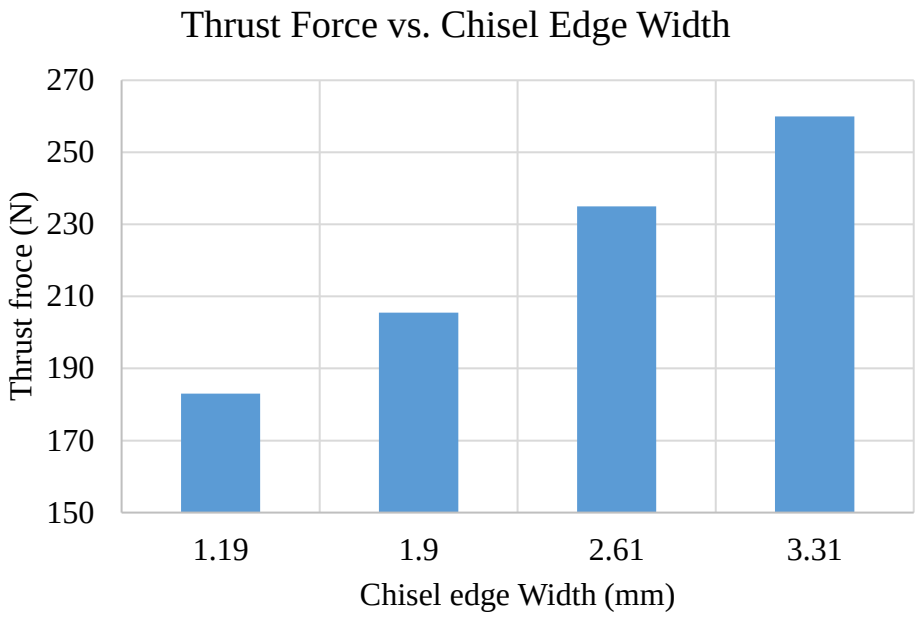

Figure 3-12 Effect of Chisel edge Width on Thrust Force, Constant point angle and helix angle

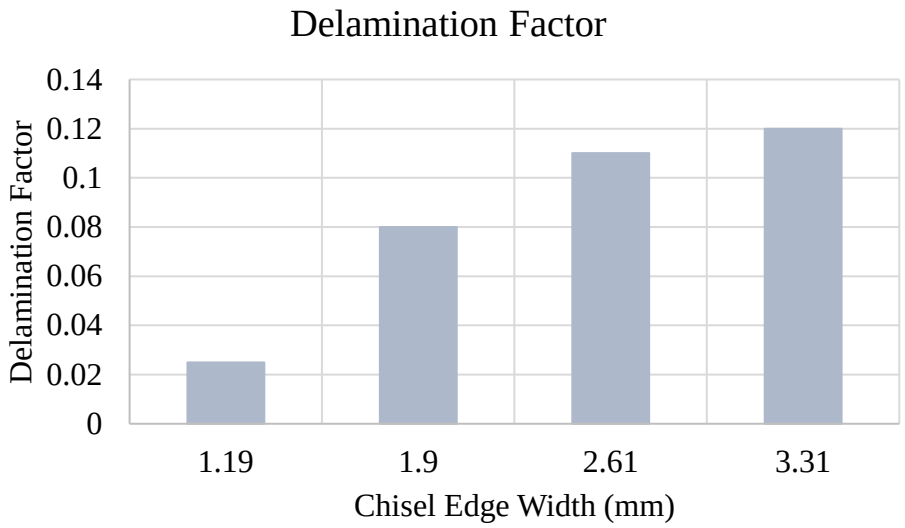

Figure 3-13 Delamination Factor study with different chisel edge widths

It is recommended by manufacturers to drill laminates and hard plastics with lower helix angle, and here in this study also the drill bit with the lowest Helix angle has the lowest delamination factor.

Comprehending the damage progression and mechanism in drilling is one of the crucial concepts of CFRP machining at this time. The presented FE simulation, takes into the account cutting energy as total of the surface energy and friction loss considering different modes of fracture and damage defects in the unidirectional CFRP and estimated the thrust force with high accuracy. The intensity of the damages surface after drilling was predicted by the designed Finite Element Model and agrees well with experiment results from the literature review. The results of simulations provided in this section, recommend a drill bit to be small in chisel edge width, small in helix angle, and 135 degrees in point angle. Choosing a suitable drill bit is crucial for the experimental analysis in the next chapter and also as a recommendation for drilling process to minimize delamination [62].

Chapter 4. Experimental Investigation of Drilling Woven Composites

Carbon fiber reinforced polymers (CFRP) have phenomenal mechanical properties such as corrosion resistance and a high strength-to-weight ratio. As a result, the use of composites in new aircrafts has reached up to 50% [64]. Drilling is one of the most common processes where the rotating movement of the drill bit cuts the material and causes a defect called delamination in composites. This defect decreases the strength and the reliability of the laminated structure [65], [66].

This current investigation aims at extending the unidirectional analytical model proposed in [67] to include a typical 2x2 twill composite shown in Figure 4-1. Design of experiments (DOE) is utilized to conduct three main phases of analysis:

- Phase one: finding a correlation relating the thrust force and the feed rate
- Phase two: investigating the chisel edge width effect on the total thrust force and updating a previous analytical model [67] accordingly
- Phase three: utilization of the effect of feed rate scheduling to minimize delamination in 2x2 twill composite

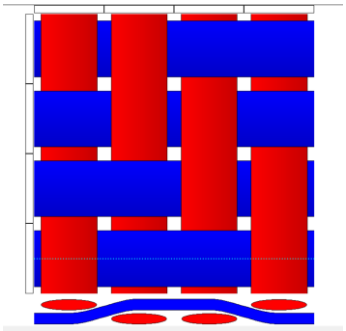

Figure 4-1. 2x2 Twill Composite

4.1 Proposed Analytical Model

Composites as inhomogeneous laminates are different from isotropic materials where each lamina is made of aligned woven carbon fibers in the epoxy matrix. Every single lamina reinforced with fabric has high stiffness and strength in two perpendicular directions. Equation (55) illustrates the load-strain equation for a laminate defined by classical plate theory (CPT) [42].

$$\begin{bmatrix} N_x \\ N_y \\ N_{xy} \\ M_x \\ M_y \\ M_{xy} \end{bmatrix} = \begin{bmatrix} [A_{i,j}(x,y)][B_{i,j}(x,y)] \\ [B_{i,j}(x,y)][D_{i,j}(x,y)] \end{bmatrix} \begin{bmatrix} e_x \\ e_y \\ e_{xy} \\ \kappa_x \\ \kappa_y \\ \kappa_{xy} \end{bmatrix} \tag{55}$$

and,

$$A_{i,j}(x,y), B_{i,j}(x,y), D_{i,j}(x,y) = \int_{-h/2}^{h/2} (1, z, z^2).\bar{Q}_{i,j}(x,y)dz \tag{56}$$

The stiffness matrix components are calculated with Equation (56). To understand and analyze the composite materials, the martial as a combination of a repetitive identical small unit cell is considered. To define the geometry of the Repetitive Unit Cell (RUC), the following geometry characteristics are introduced as illustrated in Figure 4-2[68]:

- h_f , h_w, h_m thicknesses of fill, warp, matrix (see Figure 4-2).
- a_f , a_w widths of fill and warp widths
- g_f , g_w the gaps between tows

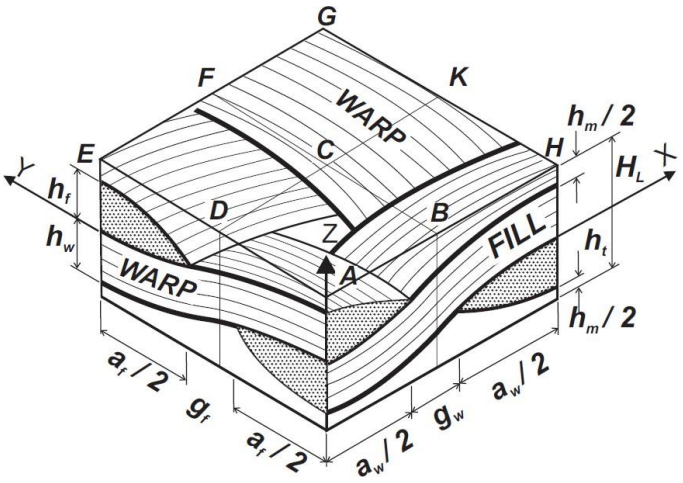

Figure 4-2. Repetitive unit cell (RUC) [68]

The total stiffness parameters E_x, E_y, G_{xy}, ν_{xy} of the laminate are considered by assembling the stiffness of all the elements in the RUC. The strain energy of RUC can be used for deriving the equivalent laminate elastic constants from the elastic properties. This is an approximation because the RUC is inhomogeneous, therefore certain elements might deform more when a load N_x, N_y, N_{xy} is considered. The iso-strain assumption is only used for elastic constants, and it is not suitable for stress analysis and failure. To simplify, the iso-strain assumption [69] is used to calculate the stiffness matrix of the laminate, as provided in Equations below.

$$[A] = \frac{4}{(a_f + g_f)(a_w + g_w)} \int_0^{\frac{(a_w+g_w)}{2}} \int_0^{\frac{(a_f+g_f)}{2}} [A(x,y)]dxdy \tag{57}$$

$$[B] = \frac{4}{(a_f + g_f)(a_w + g_w)} \int_0^{\frac{(a_w+g_w)}{2}} \int_0^{\frac{(a_f+g_f)}{2}} [B(x,y)]dxdy \tag{58}$$

$$[D] = \frac{4}{(a_f + g_f)(a_w + g_w)} \int_0^{\frac{(a_w+g_w)}{2}} \int_0^{\frac{(a_f+g_f)}{2}} [D(x,y)]dxdy \tag{59}$$

The same procedure is followed for [B] and [D] matrices in the classical plate theory. Up to this point, the stiffness matrix is adjusted to accommodate the twill

composite, with unique properties ready for use in machining process modeling. When drilling a 2x2 twill composite, the delamination area starts as a circle and grows to a larger one in the last layer of drill exit; i.e. forming a deformation cone

To predict the critical thrust force, the delamination area formed by drilling is studied by following the principle of virtual work such that potential energy variation plus the energy dissipated by delaminated parts is equal to generated work by the external forces. With the help of the plate theory [44], the stress-strain relation is defined in Equation (60), using κ the radii of curvature.

$$\kappa = \begin{Bmatrix} \kappa_x \\ \kappa_y \\ \kappa_{xy} \end{Bmatrix} = \begin{Bmatrix} -\partial^2\delta/\partial x^2 \\ -\partial^2\delta/\partial y^2 \\ -2\,\partial^2\delta/\partial x\,\partial y \end{Bmatrix} \tag{60}$$

The flexural behavior as a relation between the radii of curvature to the D matrix which is also called flexural stiffness obtains the unit moments as in Equation (61) :

$$M_{total} = \begin{Bmatrix} M_{xx} \\ M_{yy} \\ M_{xy} \end{Bmatrix} = \begin{bmatrix} D_{11} & D_{12} & D_{16} \\ D_{12} & D_{22} & D_{26} \\ D_{16} & D_{26} & D_{66} \end{bmatrix} \begin{Bmatrix} \kappa_x \\ \kappa_y \\ \kappa_{xy} \end{Bmatrix} \tag{61}$$

M_{xx} is resultant moment per unit length of y coordinate, M_{yy} is resultant moment per unit length of x coordinate and M_{xy} is the twisting moment caused by shear stresses perpendicular to the x-axis [45]. Considering only bending, due to an out-of-plane load and taking into account M_{total}, Equation (62), the total amount of the unit moments, the equilibrium equation of a plate will be as in Equation (63).

$$M_{total} = [D]\kappa \tag{62}$$

$$\kappa^T M_{total} = -q \tag{63}$$

The delamination area: for a 2x2 twill laminate at any ply, a circular area for the layer that drill bit primarily makes contact can be assumed. However, the diameter of the circle in the direction of the fibers will grow as the drill bit goes further toward the exit

ply. Eventually, the delaminated area at the exit ply is also circular. Therefore, the ellipticity ratio, η, remains 1.

Boundary conditions: In this study, a clamped-clamped boundary condition is assumed. In reality, as studied in the recent papers [47], [48] the boundary condition is between clamped and simply-supported nearly to be clamped.

Crack propagation modes: The study in [49] explained that applying the proposed mixed-mode criterion shows a solid prediction of the resultant release energy rate during drilling of CRFP, Equation (64). G_{IC} and G_{IIC} are the energy release rates in the first and second modes of fracture [6, 36].

$$G_C = G_{IC} + (G_{IIC} - G_{IC})\beta^{\zeta} \tag{64}$$

The first mode of fracture is typically the major mode for the crack propagation; however, a coupling occurs due to the stress and displacement near the crack area, with changed plies orientation. Therefore release energy rate G_c contains two failure modes

Critical thrust force: As LEFM (Linear Elastic Fracture Mechanics) describes, tooth movement $d\delta_o$, times the drilling thrust force P equals to work used up in the plate deflection and spreading the crack, Equation (65).

$$Pd\delta_0 = GdA + dU \tag{65}$$

Equations (66) to (67) define the deflection of a circular plate with a radius of a and clamped-clamped boundary conditions under q as a distributed load:

$$\delta_L = (\delta_o)_L(1 - \frac{x^2}{a^2} - \frac{y^2}{a^2})^2 \tag{66}$$

$$(\delta_0)_L = \frac{q = q_0 x}{D_L} \tag{67}$$

According to [50], for a clamped circular plate with a clamped edge and bent by linearly varying pressure, the deflection constant D_L is as follows:

$$D_L = (\frac{120D_{11} + 32(D_{12} + 2D_{66}) + 24D_{22}}{a^4}) \tag{68}$$

For calculation of the deflection of a circular plate under point load illustrated in Equations (13-15), the same process has been done.

$$\delta_c = (\delta_0)_c(1 - \frac{x^2}{a^2} - \frac{y^2}{a^2})^2 \tag{69}$$

$$(\delta_0)_c = \frac{P_c}{D_c} \tag{70}$$

$$D_c = \pi ab(\frac{6D_{11} + 6(D_{12} + 2D_{66}) + 6D_{22}}{a^4}) \tag{71}$$

By introducing γ, the chisel edge ratio, center point thrust force, and linearly distributed thrust force are expressed as follows:

$$P_c = \gamma P_{total} \tag{72}$$

$$P_L = (1 - \gamma)P_{total} \tag{73}$$

The center point thrust force represents the chisel edge force, spreading the material and applying pressure, while the linearly distributed thrust force represents the cutting lips, cutting the material as the drill bit rotates. The same notation order will help to calculate the total virtual work of the external loads as expressed in Equation (20) follows:

$$W_{total} = W_c + W_L \tag{74}$$

Equations (75) and (76) represent [41], the virtual work done by the external loads corresponding to the work of (q_L), and (q_c).

$$W_L = \int_{-a}^{a}\int_{-a}^{a} \delta_L q_L dxdy \tag{75}$$

$$W_c = \int_{-a}^{a}\int_{-a}^{a} \delta_c q_c dxdy \tag{76}$$

As $q_L = q_o x$, the linear distributed load, and $q_c = P_c/\pi a^2$, concentrated load. Also, the distributed portion of the thrust force (P_L), has a constant named, linearly distributed load constant which is shown with q_o and is expressed as:

$$P_L = \int_0^a \pi(2a)(q_o x)dx \tag{77}$$

By solving Equation (77), the linearly distributed load constant is:

$$q_o = \frac{P_L}{\pi(a^3)} \tag{78}$$

The strain energy of the delaminated area as shown in Equation (80), contain strain components defined by the curvature radii

$$\varepsilon = \begin{Bmatrix} \varepsilon_x \\ \varepsilon_y \\ \varepsilon_{xy} \end{Bmatrix} = z \begin{Bmatrix} \kappa_x \\ \kappa_y \\ \kappa_{xy} \end{Bmatrix} \tag{79}$$

$$U = \frac{1}{2}\int < \varepsilon, \sigma > dV = \frac{1}{2}\int \varepsilon^T \sigma dV \tag{80}$$

Incorporating Equation (79) into Equation (80) can be also written as:

$$U = \frac{1}{2}\int [z\kappa]^T [Q][z\kappa] dV \tag{81}$$

$$D_{ij} = \sum_{k=1}^{n} (\bar{Q}_{ij})(\frac{z_k^3 - z_{k-1}^3}{3}) \tag{82}$$

Considering Q_{ij} the bending stiffness terms and incorporating the theory of laminates and the bending stiffness matrix, D_{ij}, calculated in Equation (82), and assessing the integral term over the laminate thickness, the strain energy of the delaminated area can be expressed as follows:

$$U = \frac{1}{2}\int [\kappa]^T [D][\kappa]\, dS \tag{83}$$

with incorporating Equation (62),

$$U = \frac{1}{2}\int \int [\kappa]^T M_{total}\, dxdy \tag{84}$$

The total strain energy of the area is the sum of the strain energy due to linearly distributed load and the strain energy due to center point load, Equation 29. For further calculation of the strain energies, δ_L and δ_c, according to Equations (66) and (69) are included as the deflections of the area, respectively.

$$U_{total} = U_c + U_L \tag{85}$$

$$U_L = \frac{1}{2}\int_{-a}^{a}\int_{-a}^{a} [\kappa(\delta = \delta_L)]^T M_{total} \quad dxdy \tag{86}$$

$$U_c = \frac{1}{2}\int_{-a}^{a}\int_{-a}^{a} [\kappa(\delta = \delta_c)]^T M_{total} \quad dxdy \tag{87}$$

Delamination energy, U_d, is concluded by multiplying the total critical energy release rate, G_C, by the damaged area surface.

With previous calculations and assumptions, Equation (92) predicts the critical thrust force. In Appendix B more details about the constants in the thrust force equation can be found.

$$\partial W = \partial U + \partial U_d \tag{88}$$

Delamination energy, U_d, is concluded by the total critical energy release rate, G_C, times the damaged surface area as provided in Equation 55.

$$U_d = G_C \pi a^2 \tag{89}$$

The increase in delamination area can be calculated as shown in Equation 56:

$$\partial(Area) = \pi(a + \partial a)(a + \partial a) - \pi a^2 = 2\pi a.\partial a \tag{90}$$

Therefore, the variation of delamination strain energy is:

$$\partial U_d = 2G_C \pi a \partial a \tag{91}$$

On the other hand, drill bit geometry has an important role in calculating the total thrust force [67]. The point load portion of the thrust force is representing the chisel edge force and a linearly distributed load is used to model the cutting lip force (see Figure 4-3).

$$P = D_c D_L a^4 \left(\frac{\gamma D_L - D_I}{D_{II}}\right) \tag{92}$$

Based on previous calculations and assumptions, to predict the critical thrust force in Equation (58) can be represented by High-Speed Steel (HSS) with a point angle of 135^o and black oxide finish and 1/2, 3/8, 1/4, 1/8 inches in diameter (see Figure 4-4).

Where γ is the ratio of chisel edge indentation force to the total thrust force. D_I and D_{II} are analytical constants extracted from the predicted Equation. D_c and D_L are deflection constants for chisel edge and cutting lips respectively [67]. Thus, knowing the composite plate stiffness matrix and plate deflection the critical thrust force can be estimated by strain energy methods.

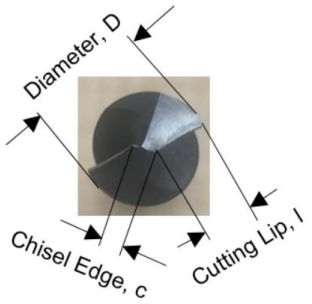

Figure 4-3. Chisel edge, cutting lips, and diameter of the drill bit illustration

4.2 Experimental Setup and Analysis

Figure 4-5 illustrates a typical experimental setup utilized in this investigation. The composite plate is mounted on plywood, pre-drilled for each hole with a 20 % bigger hole in order to minimize the bending effect, as shown in Figure 4-6. In this

work, HAAS three-axis CNC machine is utilized. The composite plate and plywood layer are placed on top of the KISTLER Dynamometer Type 9255C which is connected to KISTLER Dual Mode charge Amplifier (i.e. Type 5010B and KISTLER Disturber Box Type 5407A).

The schematic illustration of the setup can be seen in Figure 4-7. The used composite material is a twill 2x2 composite and its mechanical properties are provided in Table 4-1. The drill bits chosen for this experiment are High-Speed Steel (HSS) with a point angle of 135^{o} and black oxide finish and 1/2, 3/8, 1/4, 1/8 inches in diameter (see Figure 4-4). The experiment was repeated twice for each feed rate and the average data is reported.

Figure 4-4 Drill bits utilized in the experiments, 1/2, 3/8, 1/4, 1/8 inches in diameter

Figure 4-5. Composite plate drilling set up

Table 4-1 Mechanical Properties of the selected composite

Composite Material	E_1 (GPa)	E_2(GPa)	G_{12}(GPa)	ν12	v_f	Ply Thickness	Ply Orientation
woven carbon plate	127	13.7	4.14	0.3	0.6	0.725	Twill 2x2

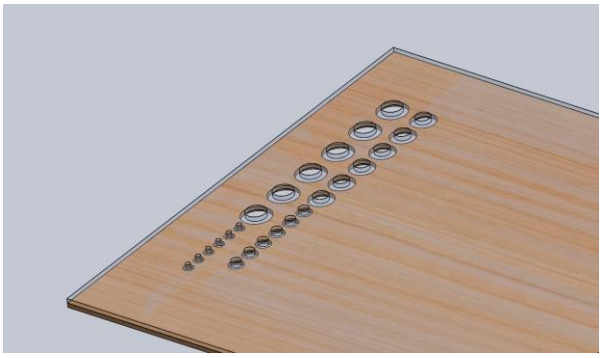

Figure 4-6. Plywood base and composite 3D model with pre-drilled holes 20% bigger than the target holes

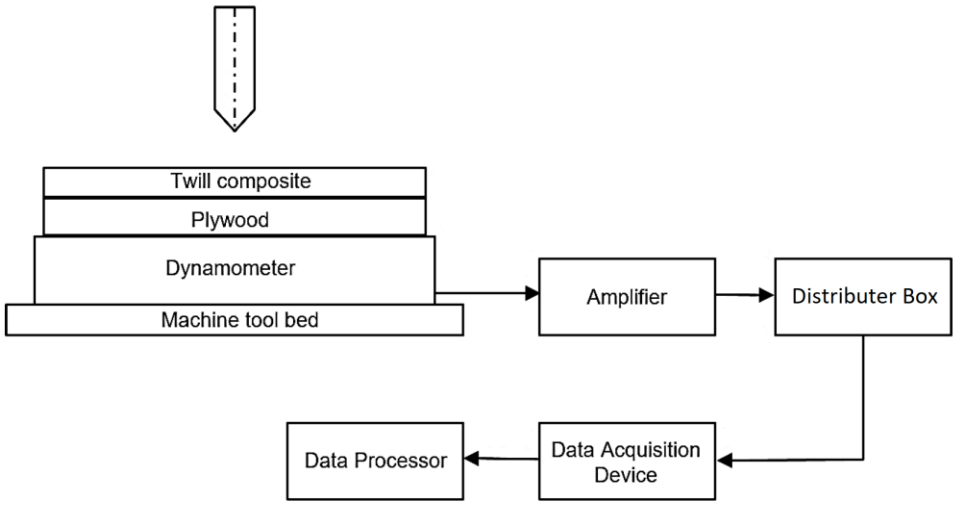

Figure 4-7. Schematic view of the composite drilling setup

The main targets of this phase are to:

- Verify the analytical modeling designed for twill composites
- Correlate the drilling thrust force to the feed rate

As explained in previous work for metals using standard, conventional twist drill curve fitting can be used to discover a correlation relating thrust force and feed rate such that [14]:

$$\frac{P}{d^2 H_B} = K_1 \frac{f^{0.8}}{d^{1.2}} + K_2 (\frac{c}{d})^2 \tag{93}$$

This equation includes drill diameter, d, Brinell hardness number, H_B, and

chisel edge width, c. The empirical constants K_1 and K_2 depend on the tool geometry and the workpiece being cut. The non-dimensional plot of thrust force versus feed rate facilitates obtaining the empirical constants. The empirical constants in Equation (93) are found with a regression line in agreement with the measured drilling thrust force in the experiments. Similarly, a set of experiments is designed to achieve a comparable relation for composites. Hence, the stiffnesses are a function of the thicknesses of the plies pushed out by the drill in the interpretation of critical thrust force and correlated feed rate. It is conventional to select the drilling feed rate based on the diameter of the drill bit but independent of the drill material. The flutes of a drill bit can sweep out chip volume proportionate to the diameter of the drill bit as provided in Equation (94),

$$f = \frac{D}{65} \tag{94}$$

For example, for a one-inch diameter drill would have about 0.015 i.p.r (0.38 mm/rev) for the feed rate [70].

To observe how the width of the chisel edge affects the total feed rate a machining test was conducted. The laminate is pre-drilled with a using drill bit which diameter is equal to the chisel width of the main drill bit. Afterward, a hole using the original drill bit is machined. Therefore, the entire thrust forced measured is now the primary cutting force at the lips. This step is repeated with several holes at different feed rates. The experimentally measure the ratio of chisel edge force to the total thrust force, γ, is now used to predict the cutting force in Equation (92).

The option of drilling the composites with a low feed rate to maintain the thrust force below a critical value is always an option, but it would be time-consuming (less productivity) with the possibility of epoxy damages. An alternative is to develop an optimal feed rate scheduling to ensure a lower the feed rate in the last few layers. The critical feed rates are calculated concerning the correlated critical thrust force (see

Equation (93). To examine the validity of feed rate scheduling, the critical thrust forces for the last four layers are analytically obtained and in the next step, the critical feed rate for each layer is calculated using Equation (93). Following this strategy, the drilling feed rate is progressively decreasing as the tool approaches the exit point.

Table 4-2. Design of Experiments

Layer	Critical Thrust Force (analytically)	Critical Feed Rate Eq. (93)
Layer 1 (Exit)	P_1	f_1
Layer 2	P_2	f_2
Layer 3	P_3	f_3
Layer 4 (Entrance)	P_4	f_4

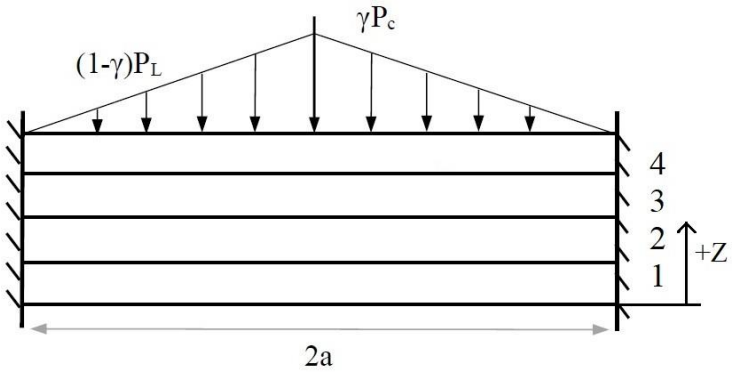

Figure 4-8. Composite workpiece numbered lay-up and force distribution

4.3 Results and Discussions

Table 4-3 illustrates the measured thrust force when using four drill diameters and six different feed rates. The average measured thrust force of three different tests, while the drill is fully engaged, has been calculated, and the effect of feed rate on the thrust force is presented in Figure 4-9*: Thrust Force vs. Feed Rate*as an observation, the measured thrust force increases as the feed rate ascends independently of the drill bit size. The values of the non-dimensional thrust force (T/d^2H_B) are plotted versus (f

$^{0.8}/d^{1.2}$) in Figure 4-10 under different process parameters. The purpose of non-dimensional plotting is to correlate the drilling thrust force to the feed rate independent of the drill bit diameter.

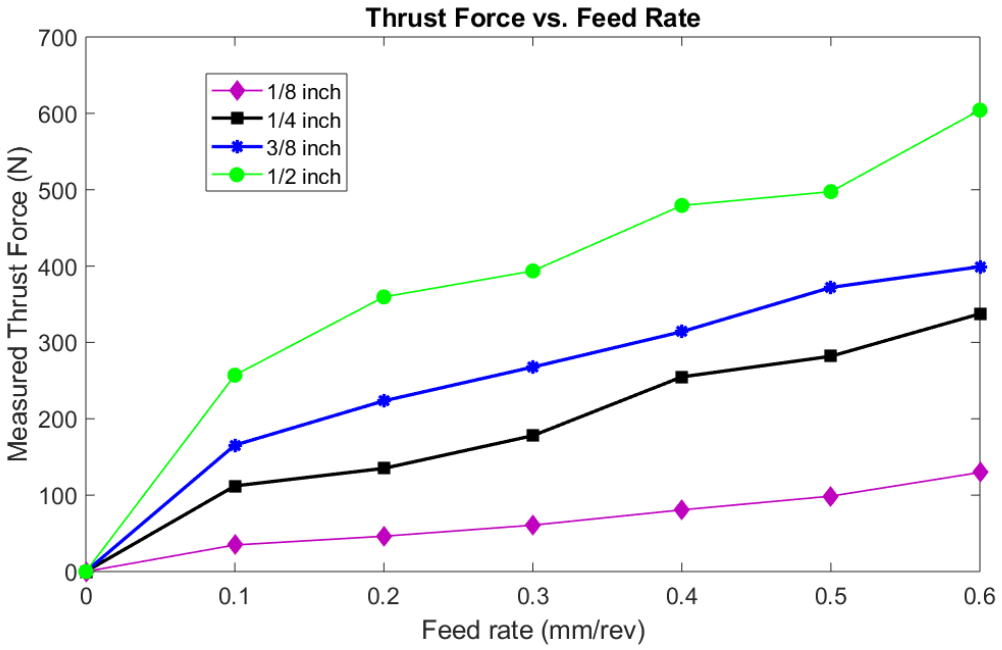

Figure 4-9: Thrust Force vs. Feed Rate

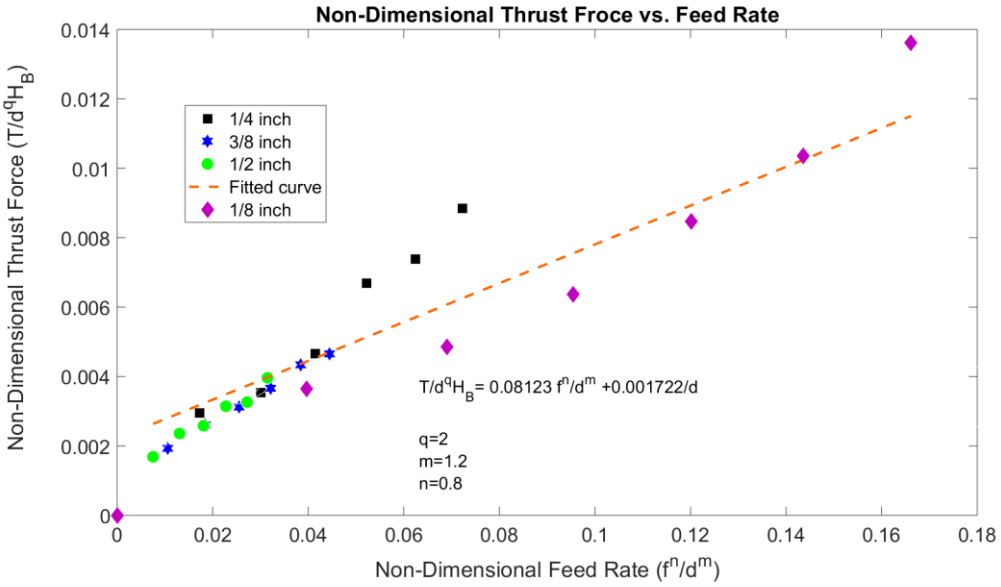

Figure 4-10. Non-Dimensional Thrust Force vs. Feed Rate

Table 4-3. Measured thrust force results

Run	Feed rate(mm/rev)	Drill diameter (inch)	Measured thrust force (N)
1	0.1	1/8	34.76
2	0.1	1/4	112.12
3	0.1	3/8	165.55
4	0.1	1/2	257.11
5	0.2	1/8	46.27
6	0.2	1/4	135.12
7	0.2	3/8	223.51
8	0.2	1/2	359.62
9	0.3	1/8	60.74
10	0.3	1/4	177.94
11	0.3	3/8	267.79
12	0.3	1/2	393.64
13	0.4	1/8	80.75
14	0.4	1/4	254.90
15	0.4	3/8	314.06
16	0.4	1/2	479.33
17	0.5	1/8	98.72
18	0.5	1/4	281.91
19	0.5	3/8	372.03
20	0.5	1/2	497.43
21	0.6	1/8	129.78
22	0.6	1/4	337.45
23	0.6	3/8	399.16
24	0.6	1/2	604.21

Equation (95) correlates the non-dimensional thrust forces to the non-dimensional feed rate.

$$\frac{T}{d^2 H_B} = 0.08123 \frac{f^{0.8}}{d^{1.2}} + \frac{0.001722}{d} \quad (95)$$

To verify the practicality of the correlated equation between thrust force and feed rate, Equation (95) is examined with the data reported in previous work [66]. In this previous study, the critical thrust force is calculated as a function of feed rate and drill bit geometry. The material chosen in the experiment was a woven CFRP laminate with 2 mm thickness and 5 mm drill bit. Three feed rates of 0.05, 0.075, and 0.1 mm/rev were used, and the thrust forces were experimentally and analytically reported. The data calculated in Equation (95) showed a reasonable agreement with the data reported in the previous study [66], with accuracy ranges from 87.61% up to 97.39% as can be seen in Table 4-4.

Table 4-4: Results verification

Feed rate (mm/rev)	Experiments by [66]Force (N)	Predicted thrust force (N) by [66]	Correlation Force (N) Equation (95)	Accuracy (%)
.05	53.45	50.14	60.07	87.61
.075	73.86	74.11	75.79	97.39
.1	90.61	97.13	84.86	93.65

The ratio of chisel edge force to the total thrust force is also investigated. The question here is how the width of the chisel edge affects the chisel edge ratio, γ. Thus, an experiment has been performed; (a) with drilling a pilot hole using drill diameter equal to the chisel edge width, and (b) drilling with the original drill (i.e. this time only cutting lips are engaged, see Figure 4-3 and Figure 4-11).

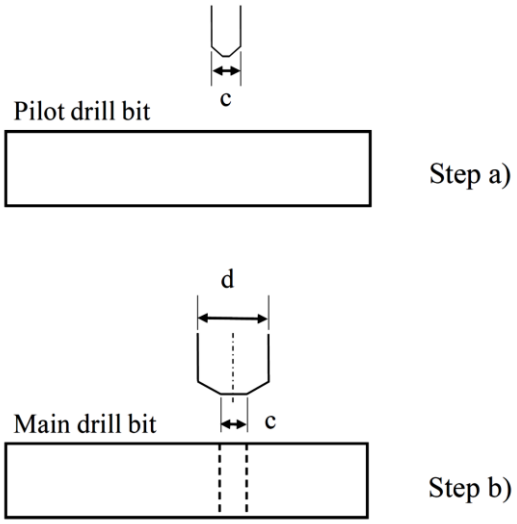

Figure 4-11 Step a) drilling the pilot holes with the same diameter as chisel edge Step b) drilling the second holes with the main diameter of the drill bit, only cutting lips are engaged.

This is a first attempt in the open literature to accurately determine the value of γ, and accordingly to provide more accurate modeling to the thrust force when drilling woven composites. The value of the chisel edge thrust force can be estimated by subtracting the cutting lip thrust force from the total drilling thrust force. The data are reported in Table 4-6 for four drill bits of 1/2 inch, 3/8 inch, 1/4 inch, and 1/8 inch in diameter. Hence, for the 1/4-inch drill bit, the point angle is 135^{o}, the chisel edge width is 0.075 inch and the calculated γ is found to be 70%. The complete drill bits characteristics are given in Table 4-5.

Table 4-5. Drill bits characteristics

D (inch)	Chisel Edge Width (inch)	Point Angle (degrees)	c/D (%)
1/2	0.110	135	26.6
3/8	0.103	135	27
1/4	0.075	135	30
1/8	0.047	135	33.6

Initially, γ (i.e. the ratio of chisel edge force to the total thrust force) was selected to be 50%. Now, the analytical model is updated with the new optimal γ. As shown in Table 4-6, the chisel edge thrust force is more than 50% of the total drilling thrust force. Besides, the proposed model showed a good agreement when compared to the measured total force. It should be stated here that the chisel edge pushes away the material through the indentation mechanism (see Figure 4-12) then it will be removed by the cutting lips. This process affects the total thrust force in a major way, more than previously expected.

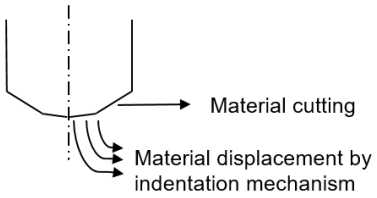

Figure 4-12. Drilling mechanism through the chisel edge and the cutting lips

Table 4-6. The contribution of the chisel edge width on the total thrust force

D (inch)	f (mm/rev)	Measured Total Force (N)	Cutting Lip Force (N)	Chisel Edge Force (N)	γ (%)
1/2	0.35	436.49	152.77	283.72	65
3/8	0.35	290.92	96.01	194.91	67
1/4	0.35	216.42	64.93	151.49	70
1/8	0.35	70.75	19.10	51.65	73

After calculating the value of γ, the feed rate scheduling is set to be tested. As explained in the previous section, the feed rate schedule will be performed for the last four layers (i.e. decreasing the feed rate for each layer to minimize the delamination). The appropriate feed rates are estimated from Equation (95) based on the critical thrust force predicted from the analytical model adjusted to 2x2 twill composite. The drill bits

are HSS with a black oxide finish. The reason for selecting this type of drill bit is to investigate if the feed rate scheduling is effective.

The estimated feed rates are reported in Table 4-7, Table 4-8, Table 4-9, and Table 4-10 for 1/2 inch, 3/8 inch, 1/4 inch, and 1/8 inch drill bits, respectively.

Table 4-7. The developed feed rate scheduling for each layer in case of 1/2inch drill bit

Layer (as shown Figure 4-8)	Thrust Force (N)	Feed rate (mm/rev)
Layer 1 (Exit)	65.47	0.024
Layer 2	178.24	0.069
Layer 3	315.21	0.157
Layer 4 (Entrance)	450.60	0.364

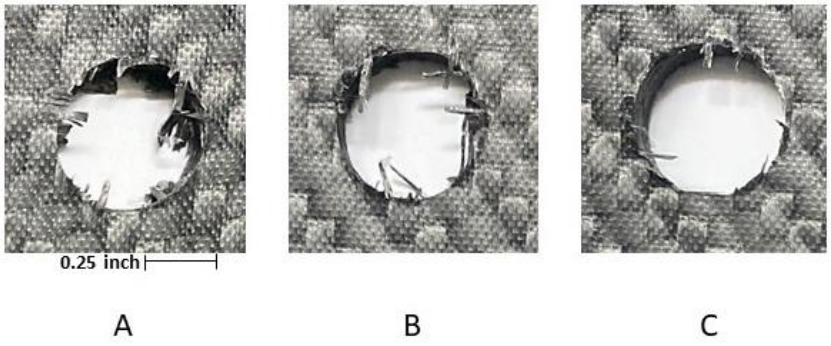

Figure 4-13 The damaged area for 1/2 inch drill bit; A) no feed rate scheduling (Equation 10), B) initial $\gamma = 50\%$, C) calculated $\gamma = 65\%$

When using 1/2 inch drill bit diameter, Figure 4-13-A illustrates a severe case of delamination since it was drilled without any feed rate scheduling and the feed rate was selected according to Equation (94).

Figure 4-13-B and Figure 4-13-C show much less delaminated damages when the feed rate schedule was applied.

However, comparing Figure 4-13-B and Figure 4-13-C, case C has less

delamination due to changing the value of γ from 50% to 65% and applying feed rate scheduling. Feed rate scheduling resulted in a round drilled hole with minimum delamination.

Table 4-8. The developed feed rate scheduling for each layer in case of 3/8 inch drill bit

Layer	Thrust Force (N)	Feed rate (mm/rev)
Layer 1 (Exit)	55.06	0.032
Layer 2	149.8	0.094
Layer 3	264.88	0.307
Layer 4 (Entrance)	378.63	0.517

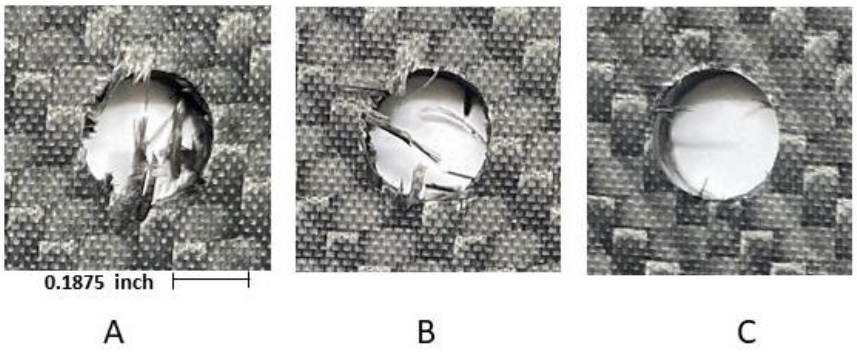

Figure 4-14 The damaged area for 3/8 inch drill bit; A) no feed rate scheduling (Equation 10), B) initial γ = 50%, C) calculated γ = 67%

Using 3/8 inch drill bit diameter as in Figure 4-14-A also causes delamination using Equation (94). Comparing between Figure 4-14-B and Figure 4-14-C, case C has less delamination due to changing the value of γ from 50% to 67% and applying feed rate scheduling.

Table 4-9. The developed feed rate scheduling for each layer in case of 1/4 inch drill bit

Layer	Thrust Force (N)	Feed rate (mm/rev)
Layer 1 (Exit)	43.096	0.038
Layer 2	117.14	0.125
Layer 3	207.07	0.340
Layer 4 (Entrance)	295.97	0.515

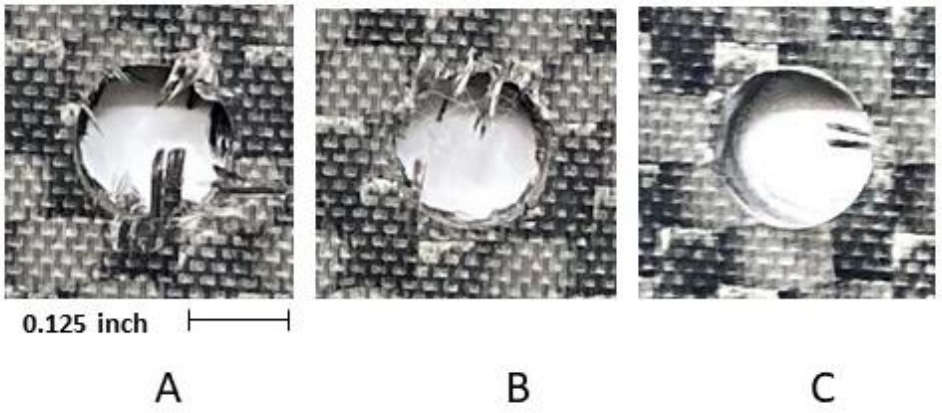

Figure 4-15. The damaged area for 1/4-inch drill bit; A) no feed rate scheduling (Equation 10), B) initial $\gamma = 50\%$, C) optimal $\gamma = 70\%$

Similarly, for the 1/4 inch drill bit, Figure 4-15-A is the result of drilling with no feed rate scheduling where the used feed is calculated using Equation (94). Figure 4-15-B shows the delamination defect with the γ ratio of 50%, while Figure 4-15-C is the final result of minimizing delamination when using the $\gamma = 70\%$. It was found that feed rate scheduling significantly improves the quality of the drilled hole and minimizes the delamination visibly. Hence, in the last layers, as the drill gets closer to the exit, there is less material to cut and less strength against the thrust force. In other words, decreasing the feed rate results in the drilling thrust force to adapt to the remaining material strength and reducing the damage.

Table 4-10. The developed feed rate scheduling for each layer in case of 1/8 inch drill bit

Layer	Thrust Force (N)	Feed rate (mm/rev)
Layer 1 (Exit)	29.32	0.064
Layer 2	79.52	0.39
Layer 3	140.51	0.451
Layer 4 (Entrance)	200.78	0.613

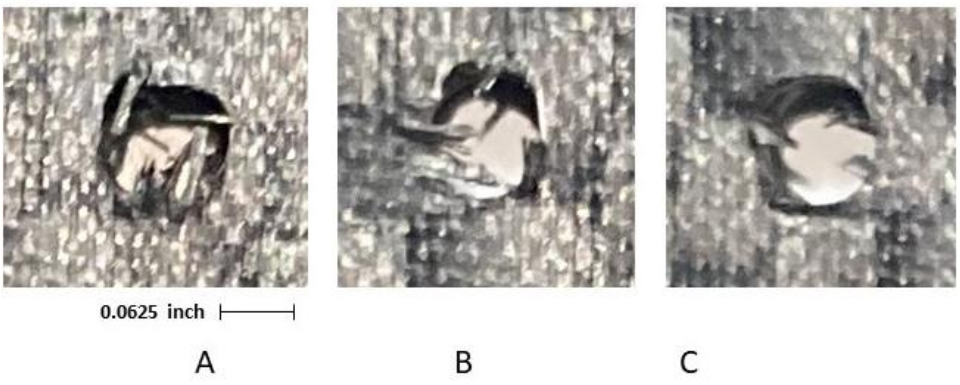

Figure 4-16. The damaged area for 1/8-inch drill bit; A) no feed rate scheduling (Equation 10), B) initial $\gamma = 50\%$, C) optimal $\gamma = 73\%$

For 1/8 inch drill bit, Figure 4-16-A is the result of drilling using Equation (94). Figure 4-16-B shows the delamination defect with the γ ratio of 50%, while Figure 4-16-C is the final result of minimizing delamination when using the $\gamma = 73\%$. It was found that feed rate scheduling significantly improves the quality of the drilled hole and minimizes the delamination visibly.

4.4 Recommended Feed Rate Scheduling Guidelines

A series of tables can be designed as guidelines for choosing suitable drilling

feed rates. The proposed feed rate table would be designed based on the ply thickness, hole diameter, and chosen material. This analytical model and the correlated feed rate equation can be extended to any type of woven composite, composite ply thickness, and drill bit size.

Table 4-11. Feed rate scheduling guideline for drill bit size 1/8 inch

Ply thickness (mm)	f_1 (mm/rev)	f_2(mm/rev)	f_3(mm/rev)	f_4(mm/rev)
0.5	0.032526	0.15013	0.325537	0.520781
0.6	0.051111	0.2185	0.466587	0.742224
0.7	0.072993	0.298059	0.630319	0.999046
0.8	0.098069	0.388552	0.816258	1.290525
0.9	0.12626	0.489775	1.024008	1.616058
1	0.157503	0.601552	1.253231	1.975125

Table 4-12. Feed rate scheduling guideline for drill bit size 1/4 inch

Ply thickness (mm)	f_1 (mm/rev)	f_2(mm/rev)	f_3(mm/rev)	f_4(mm/rev)
0.5	0.019572	0.108161	0.242118	0.391784
0.6	0.033337	0.160275	0.350209	0.561814
0.7	0.049736	0.221087	0.475864	0.759203
0.8	0.068656	0.290385	0.618699	0.983374
0.9	0.09002	0.367995	0.778396	1.233851
1	0.113771	0.453777	0.954686	1.510224

Table 4-13. Feed rate scheduling guideline for drill bit size 3/8 inch

Ply thickness (mm)	f_1 (mm/rev)	f_2(mm/rev)	f_3(mm/rev)	f_4(mm/rev)
0.5	0.013419	0.08805	0.202249	0.330221
0.6	0.024832	0.132409	0.294652	0.475794
0.7	0.038584	0.184289	0.40219	0.644918
0.8	0.05455	0.243494	0.524522	0.837085
0.9	0.072648	0.309867	0.661367	1.051878
1	0.092819	0.383281	0.812488	1.288939

Table 4-14. Feed rate scheduling guideline for drill bit size 1/2 inch

Ply thickness (mm)	f_1 (mm/rev)	f_2(mm/rev)	f_3(mm/rev)	f_4(mm/rev)
0.5	0.009612	0.075439	0.177297	0.291738
0.6	0.019515	0.114949	0.259913	0.422065
0.7	0.031593	0.161253	0.356156	0.573573
0.8	0.045701	0.214161	0.465709	0.745799
0.9	0.06175	0.273526	0.588313	0.93836
1	0.079681	0.339228	0.723751	1.150931

Chapter 5. Conclusions and Future Work

This study focused on four substantial points to predict the critical thrust force aiming to minimize delamination caused by drilling:

(i) Unidirectional composite structures are exposed to both modes I and II, therefore a proportionate critical energy release rate is required,

(ii) Since high temperature affects the properties of unidirectional laminate composites, thermo-mechanical loads is considered

(iii) The delamination area starts as a circular area and grows into an elliptical area in the same direction as the fibers,

(iv) A portion of the thrust force is a center point load, modeling the chisel edge force, while the rest is a linearly distributed load, modeling the cutting lip force.

After demonstrating the mathematical modeling, the new analytical model for the thrust force is compared with five different analytical models from the literature review in three different sets of experiments including different composite materials, drill bits, and feed rates overall, the new analytical model improves the results by 2.80% for the first case, 11.35% in the second case, and 26.38 % in the last set of experiments. Further improvement of this delamination model to multi-directional laminates with feed rate analysis with a new set of experiments is required in the future.

With the help of Finite Element simulations, the effects of the drill bit geometry such as chisel edge width, point angle, and helix angle, on thrust force and delamination factor were discussed in detail to have a better understanding of delamination phenomena and the suitable drill bit design for drilling. In terms of the future work for this phase, incorporating new sustainable cooling techniques such as cryogenic environment can be fully discussed (investigating the cooling effect on the delamination

phenomena).

In the second phase of this study, different experiments are designed in three stages to discover a guided machining approach for drilling woven composites and obtain drilled holes with minimum delamination. An analytical model based on the drill bit geometry, delaminated area, indentation forces, cutting forces, and woven composite mechanical properties has been developed and discussed. Firstly, a correlation between the thrust force and the feed rate is established based on the conducted drilling experiments using four sizes of drill bits and six different feed rates. Secondly, the contribution of the chisel edge width on the total thrust force is investigated. The current study results in finding an optimal chisel edge ratio, (the ratio of chisel edge force to the total thrust force), and updating the analytical model concerning the drill bit size. Lastly, a feed rate scheduling approach is proposed to minimize the delamination. The goal is to control the delamination phenomena with current machining resources and commonly used drill bits through a guided machining approach. This proposed approach significantly decreases the delaminated area and fiber breakage it was observed that only scheduling the feed rate is not sufficient for minimizing the delamination. However, updating the chisel edge ratio based on the drill bit geometry results in predicting a more accurate thrust force which can sufficiently minimize the delamination. For a more practical approach, a series of tables are designed as guidelines for choosing the suitable drilling feed rates. The proposed feed rate table would be designed based on the ply thickness, the hole diameter, chosen material, and spindle speed.

Appendices

Appendix A

1. Analytical model constants for unidirectional composite

In the proposed critical model, there are two coefficients as the result of the analytical modeling code. Below, the details of these coefficients are shown.

$$D_I = (a^2\sqrt{(}(3D_l^2ab^2\gamma^2 - 12D_{22}D_c^2G_ca^6\pi^2 + 24D_{22}Dc^2G_ca^6\gamma\pi^2 + 180D_{11}D_c^2G_ca^2b^4\pi^2 + 24D_{12}D_c^2G_ca^4b^2\pi^2 + 48D_{66}D_c^2G_ca^4b^2\pi^2 + D_c^2D_lG_ca^6b^4\pi^2 - 12D_{22}D_c^2G_ca^6\gamma^2\pi^2 + 96D_{22}D_l^2G_ca^4\gamma^2\pi^2 + 480D_{11}D_l^2G_cb^4\gamma^2\pi^2 - 360D_{11}D_c^2G_ca^2b^4\gamma\pi^2 - 48D_{12}D_c^2G_ca^4b^2\gamma\pi^2 - 96D_{66}D_c^2G_ca^4b^2\gamma\pi^2 - 2D_c^2D_lG_ca^6b^4\gamma\pi^2 + 180D_{11}D_c^2G_ca^2b^4\gamma^2\pi^2 + 24D_{12}D_c^2G_ca^4b^2\gamma^2\pi^2 + 48D_{66}D_c^2G_ca^4b^2\gamma^2\pi^2 + 192D_{12}D_l^2G_ca^2b^2\gamma^2\pi^2 + 384D_{66}D_l^2G_ca^2b^2\gamma^2\pi^2 + D_c^2D_lG_ca^6b^4\gamma^2\pi^2)/(3a^5)))$$

$$D_{II} = (24D_{22}D_c^2a^6\gamma - 12D_{22}D_c^2a^6 + 180D_{11}D_c^2a^2b^4 + 24D_{12}D_c^2a^4b^2 + 48D_{66}D_c^2a^4b^2 + D_c^2D_la^6b^4 - 12D_{22}D_c^2a^6\gamma^2 + 96D_{22}D_l^2a^4\gamma^2 + 480D - 11D_l^2b^4\gamma^2 - 360D_{11}D_c^2a^2b^4\gamma - 48D_{12}D_c^2a^4b^2\gamma - 96D_{66}Dc^2a^4b^2\gamma - 2D_c^2D_la^6b^4\gamma + 180D_{11}D_c^2a^2b^4\gamma^2 + 24D_{12}D_c^2a^4b^2\gamma^2 + 48D_{66}D_c^2a^4b^2\gamma^2 + 192D_{12}D_l^2a^2b^2\gamma^2 + 384D_{66}D_l^2a^2b^2\gamma^2 + D_c^2D_la^6b^4\gamma^2)$$

Appendix B

2. Analytical model constants for twill composite

$$D_I = \sqrt{(}D_l^2\gamma^2 + 30\,D_{11}D_c^2G_ca^3\pi^2 + 12D_c^2G_ca^3\pi^2 + 6D_{22}D_c^2G_ca^3\pi^2$$
$$+\ 24D_{66}D_c^2G_ca^3\pi^2 - 60D_{11}D_c^2G_ca^3\gamma\pi^2 - 24D_{12}D_c^2G_ca^3\gamma\pi^2$$
$$- 12D_{22}D_c^2G_ca^3\gamma\pi^2 - 48D_{66}D_c^2G_ca^3\gamma\pi^2 + 72D_{11}D_l^2G_c\mathrm{a}\gamma^2\pi^2$$
$$+ 48D_{12}D_l^2G_c\mathrm{a}\gamma^2\pi^2 + 72D_{22}D_l^2G_c\mathrm{a}\gamma^2\pi^2 + 96D_{66}D_l^2G_c\mathrm{a}\gamma^2\pi^2$$
$$+ 30D_{11}D_c^2G_ca^3\gamma^2\pi^2 + 12D_{12}D_c^2G_ca^3\gamma^2\pi^2 + 6D_{22}D_c^2G_ca^3\gamma^2\pi^2$$
$$+ 24D_{66}D_c^2G_ca^3\gamma^2\pi^2)$$

$$D_{II} = (5D_{11}D_c^2a^2 + 2D_{12}D_c^2a^2 + D_{22}D_c^2a^2 + 4D_{66}D_c^2a^2 + 12D_{11}D_l^2\gamma^2 + 8D_{12}D_l^2\gamma^2$$
$$+ 12D_{22}D_l^2\gamma^2 + 16D_{66}D_l^2\gamma^2 - 10D_{11}D_c^2a^2\gamma - 4D_{12}D_c^2a^2\gamma$$
$$- 2D_{22}D_c^2a^2\gamma - 8D_{66}D_c^2a^2\gamma + 5D_{11}D_c^2a^2\gamma^2 + 2D_{12}D_c^2a^2\gamma^2$$
$$+ D_{22}D_c^2a^2\gamma^2 + 4D_{66}D_c^2a^2\gamma^2)$$

Appendix C

Symmetrical Bending Deflection for Circular Plates

Laterally loaded circular plates have a differential equation for symmetrical bending. In case of a distributed load in asymmetric manner applied on a circular plate with a centered axis perpendicular to the plate, the bent deflection surface will also appear to be symmetrical. Meaning, deflection is equal for all the equally distanced points, and it is satisfactory to consider deflections in one diametric section through the axis of symmetry (Figure C-1). The following notes are considered;

- Point O is the origin of the coordination system
- r is the radial distance of the points
- δ denoting the deflection in the descending direction
- Maximum slope can be defined as $-d\delta/dr$
- The curvature is in section rz and can be calculated by:

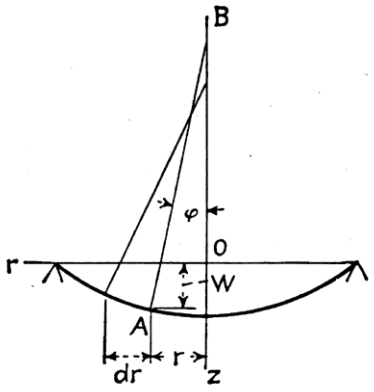

Figure C-1 Deflection in one diametric section [50]

$$\frac{1}{r_n} = -\frac{d^2\delta}{dr^2} = \frac{d\varphi}{dr}$$

Hence:

- φ shows the angle between the symmetry axis OB and the deflection surface normal

- The main curvature is $\frac{1}{r_n}$, deflection at point A

Then from the figure, we obtain,

$$\frac{1}{r_t} = -\frac{1}{r}\frac{d\delta}{dr} = \frac{\varphi}{r}$$

Having the equations above for the main curvature, it is concluded the corresponding values of the bending moments assuming the equations derived from pure bending, moments and the curvature. Therefore,

$$M_r = -D\left(\frac{d^2\delta}{dr^2} + \frac{\vartheta}{r}\frac{d\delta}{dr}\right) = D\left(\frac{d\varphi}{dr} + \frac{\vartheta}{r}\varphi\right)$$

$$M_t = -D\left(\vartheta\frac{d^2\delta}{dr^2} + \frac{1}{r}\frac{d\delta}{dr}\right) = D\left(\vartheta\frac{d\varphi}{dr} + \frac{\varphi}{r}\right)$$

where, as before, M_r and M_t signify bending moments per unit length. The moment M_r exists alongside circumferential sections of the plate.

The moments equations include one parameter φ or δ, which can be found by observing the equilibrium of an element of the plate i.e. the element $abcd$ in Figure C-2 take away from the plate by two sections ab and cd in cylindrical form and by ad and bc in diametral form. The couple on the side cd of the element is $M_r r d\theta$. The corresponding couple on the side ab is,

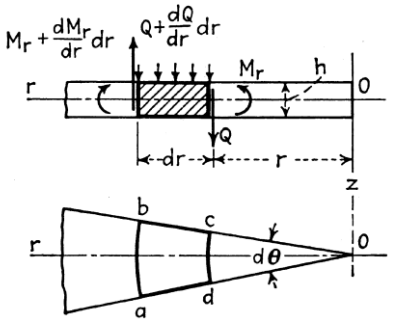

Figure C-2 abcd element [50]

$$\left(M_r + \frac{dM_r}{dr}dr\right)(r + dr)d\theta$$

The couples on the edges ad and bc of the element are each $M_t dr$ and with a resultant couple in the plane rOz equal to $M_r dr d\theta$.

Concluded by symmetry, the shearing forces acting on the element disappear on edges cd and ab of the element. Named as Q the shearing force per unit length of the radius r, the total shearing force present on the edge cd of the element is $Qrd\theta$ with corresponding force on the edge ab as,

$$\left[Q + \left(\frac{dQ}{dr}\right) dr\right](r + dr)d\theta$$

Ignoring the small dissimilarity between the shearing forces on the two opposite sides of the element, these forces give a couple in the rz plane as $Qrd\theta dr$.

Summing up the moments with suitable signs and avoiding the moment because of the external load on the element (small quantity of higher-order), the relation below of the element $abcd$ can be found,

$$\left(M_r + \frac{dM_r}{dr} dr\right)(r + dr)d\theta - M_r d\theta - M_t dr d\theta + Qr\, d\theta\, dr = 0$$

Not considering a small quantity of higher-order,

$$M_r + \frac{dM_r}{dr} r - M_t + Qr + 0$$

Substituting equations for M_r and M_t we have,

$$\frac{d^3\delta}{dr^3} + \frac{1}{r}\frac{d^2\delta}{dr^2} - \frac{1}{r^2}\frac{d\delta}{dr} = \frac{Q}{D}$$

flexural rigidity of the plate is presented as D. In case of the asymmetrically loaded circular plate, Q can be estimated by dividing the load distribution through the circle of radius r by cross section area $2\pi r$. The integration of these equations is simplified by the following form,

$$\frac{d}{dr}\left[\frac{1}{r}\frac{d}{dr}\left(r\frac{dw}{dr}\right)\right] = \frac{Q}{D}$$

With q as a function of r, to be integrated with ease in each special case.

Showing the second side of the equation as a dependent of q of the load distributed over the plate, meaning, multiplying left and right sides of the equation by the cross section $2\pi r$. Considering,

$$Q2\pi r = \int_0^r q2\pi r\, dr$$

It is concluded,

$$r\frac{d}{dr}\left[\frac{1}{r}\frac{d}{dr}\left(r\frac{dw}{dr}\right)\right] = \frac{1}{D}\int_0^r qr\, dr$$

Differentiating both sides of this equation are differentiated in respect to r and dividing by r, the final result is,

$$\frac{1}{r}\frac{d}{dr}\left\{r\frac{d}{dr}\left[\frac{1}{r}\frac{d}{dr}\left(r\frac{dw}{dr}\right)\right]\right\} = \frac{q}{D}$$

with the load q is driven as a function of r.

Appendix D

Classic Laminate Theory

For studying the strength, stiffness, and failure analysis of FRPs, the anisotropic behavior of the FRP laminate must be included. Therefore, the analysis is in the microscopic lamina level of the specific components of the composite, Reinforcing fibers, the matrix or resin and the interface layer. The following appendix is in the lamina level.

Fiber reinforced Polymers mechanical properties, influenced by the mechanical properties of its components, vary significantly and be governed by the volume fraction occupied by each component. Rules of mixtures include equations calculating the elastic properties of FRPs taking into consideration the unique properties of its components and designated volume fractions.

Stacking sequence,

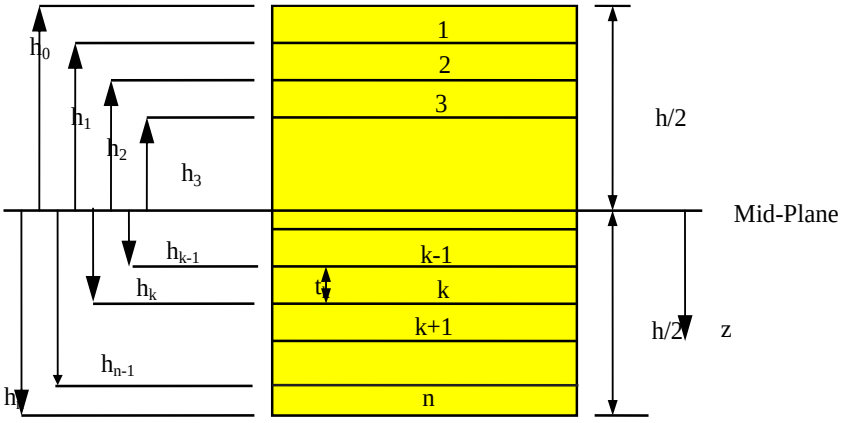

Figure D-1 coordinate locations of plies in the laminate

Stresses in a lamina in a laminate,

$$\begin{bmatrix} \sigma_x \\ \sigma_y \\ \tau_{xy} \end{bmatrix}_k = \begin{bmatrix} \overline{Q}_{11} & \overline{Q}_{12} & \overline{Q}_{16} \\ \overline{Q}_{12} & \overline{Q}_{22} & \overline{Q}_{26} \\ \overline{Q}_{16} & \overline{Q}_{26} & \overline{Q}_{66} \end{bmatrix}_k \begin{bmatrix} \varepsilon_x \\ \varepsilon_y \\ \gamma_{xy} \end{bmatrix}_k$$

$$= \begin{bmatrix} \overline{Q}_{11} & \overline{Q}_{12} & \overline{Q}_{16} \\ \overline{Q}_{12} & \overline{Q}_{22} & \overline{Q}_{26} \\ \overline{Q}_{16} & \overline{Q}_{26} & \overline{Q}_{66} \end{bmatrix}_k \begin{bmatrix} \varepsilon_x^0 \\ \varepsilon_y^0 \\ \gamma_{xy}^0 \end{bmatrix} + z \begin{bmatrix} \overline{Q}_{11} & \overline{Q}_{12} & \overline{Q}_{16} \\ \overline{Q}_{12} & \overline{Q}_{22} & \overline{Q}_{26} \\ \overline{Q}_{16} & \overline{Q}_{26} & \overline{Q}_{66} \end{bmatrix}_k \begin{bmatrix} \kappa_x \\ \kappa_y \\ \kappa_{xy} \end{bmatrix}.$$

Forces and stresses,

$$\begin{bmatrix} N_x \\ N_y \\ N_{xy} \end{bmatrix} = \int_{-h/2}^{h/2} \begin{bmatrix} \sigma_x \\ \sigma_y \\ \tau_{xy} \end{bmatrix} dz, \quad = \sum_{k=1}^{n} \int_{h_{k-1}}^{h_k} \begin{bmatrix} \sigma_x \\ \sigma_y \\ \tau_{xy} \end{bmatrix}_k dz,$$

Forces and mid-plane strains/curvatures,

$$\begin{bmatrix} N_x \\ N_y \\ N_{xy} \end{bmatrix} = \sum_{k=1}^{n} \int_{h_{k-1}}^{h_k} \begin{bmatrix} \overline{Q}_{11} & \overline{Q}_{12} & \overline{Q}_{16} \\ \overline{Q}_{12} & \overline{Q}_{22} & \overline{Q}_{26} \\ \overline{Q}_{16} & \overline{Q}_{26} & \overline{Q}_{66} \end{bmatrix}_k \begin{bmatrix} \varepsilon_x^0 \\ \varepsilon_y^0 \\ \gamma_{xy}^0 \end{bmatrix} dz$$

$$+ \sum_{k=1}^{n} \int_{h_{k-1}}^{h_k} \begin{bmatrix} \overline{Q}_{11} & \overline{Q}_{12} & \overline{Q}_{16} \\ \overline{Q}_{12} & \overline{Q}_{22} & \overline{Q}_{26} \\ \overline{Q}_{16} & \overline{Q}_{26} & \overline{Q}_{66} \end{bmatrix}_k \begin{bmatrix} \kappa_x \\ \kappa_y \\ \kappa_{xy} \end{bmatrix} z \, dz$$

Integrating terms,

$$\int_{h_{k-1}}^{h_k} dz = (h_k - h_{k-1}), \qquad \int_{h_{k-1}}^{h_k} z dz = \frac{1}{2} (h_k^2 - h_{k-1}^2),$$

Moments and mid-planes strains/curvatures

$$\begin{bmatrix} M_x \\ M_y \\ M_{xy} \end{bmatrix} = \left\{ \sum_{k=1}^{n} \begin{bmatrix} \overline{Q}_{11} & \overline{Q}_{12} & \overline{Q}_{16} \\ \overline{Q}_{12} & \overline{Q}_{22} & \overline{Q}_{26} \\ \overline{Q}_{16} & \overline{Q}_{26} & \overline{Q}_{66} \end{bmatrix}_k \int_{h_{k-1}}^{h_k} z\,dz \right\} \begin{bmatrix} \varepsilon_x^0 \\ \varepsilon_y^0 \\ \gamma_{xy}^0 \end{bmatrix}$$

$$+ \left\{ \sum_{k=1}^{n} \begin{bmatrix} \overline{Q}_{11} & \overline{Q}_{12} & \overline{Q}_{16} \\ \overline{Q}_{12} & \overline{Q}_{22} & \overline{Q}_{26} \\ \overline{Q}_{16} & \overline{Q}_{26} & \overline{Q}_{66} \end{bmatrix}_k \int_{h_{k\,1}}^{h_k} z^2\,dz \right\} \begin{bmatrix} \kappa_x \\ \kappa_y \\ \kappa_{xy} \end{bmatrix}$$

Substituting the following terms,

$$A_{ij} = \sum_{k=1}^{n} [(\overline{Q}_{ij})]_k \ (h_k - h_{k-1}),\ i = 1,2,6;\ j = 1,2,6,$$

[A] – Extensional stiffness matrix, the resultant in-plane forces vs. the in-plane strains.

$$B_{ij} = \frac{1}{2} \sum_{k=1}^{n} [(\overline{Q}_{ij})]_k \ (h_k^2 - h_{k-1}^2),\ i = 1,2,6;\ j = 1,2,6$$

[B] – Coupling stiffness matrix the force and moment to the strains and mid-plane curvatures in mid-plane coupling.

$$D_{ij} = \frac{1}{3} \sum_{k=1}^{n} [(\overline{Q}_{ij})]_k \ (h_k^3 - h_{k-1}^3), \qquad i = 1,2,6;\ j = 1,2,6.$$

[D] – Bending stiffness matrix, resultant bending moments vs. plate curvatures.

where,

$$\overline{Q}_{11} = Q_{11}c^4 + Q_{22}s^4 + 2(Q_{12} + 2Q_{66})s^2c^2$$

$$\overline{Q}_{12} = (Q_{11} + Q_{22} - 4Q_{66})s^2c^2 + Q_{12}(c^4 + s^4)$$

$$\overline{Q}_{26} = (Q_{11} - Q_{12} - 2Q_{66})cs^3 - (Q_{22} - Q_{12} - 2Q_{66})c^3 s$$

$$\overline{Q}_{16} = (Q_{11} - Q_{12} - 2Q_{66})c^3 s - (Q_{22} - Q_{12} - 2Q_{66})s^3 c$$

$$\overline{Q}_{66} = (Q_{11} + Q_{22} - 2Q_{12} - 2Q_{66})s^2 c^2 + Q_{66}(s^4 + c^4)$$

$$\overline{Q}_{22} = Q_{11}s^4 + Q_{22}c^4 + 2(Q_{12} + 2Q_{66})s^2 c^2$$

And, θ is the ply orientation, therefor,

$$c = \cos(\theta)$$

$$s = \sin(\theta)$$

$$Q_{11} = \frac{E_1}{1 - v_{21}\, v_{12}}$$

$$Q_{12} = \frac{v_{12}\, E_2}{1 - v_{21} v_{12}}$$

$$Q_{22} = \frac{E_2}{1 - v_{21}\, v_{12}}$$

$$Q_{66} = G_{12}$$

Forces, moments, mid-plane strains and mid-plane curvatures,

$$\begin{bmatrix} N_x \\ N_y \\ N_{xy} \\ M_x \\ M_y \\ M_{xy} \end{bmatrix} = \begin{bmatrix} A_{11} & A_{12} & A_{16} & B_{11} & B_{12} & B_{16} \\ A_{12} & A_{22} & A_{26} & B_{12} & B_{22} & B_{26} \\ A_{16} & A_{26} & A_{66} & B_{16} & B_{26} & B_{66} \\ B_{11} & B_{12} & B_{16} & D_{11} & D_{12} & D_{16} \\ B_{12} & B_{22} & B_{26} & D_{12} & D_{22} & D_{26} \\ B_{16} & B_{26} & B_{66} & D_{16} & D_{26} & D_{66} \end{bmatrix} \begin{bmatrix} \varepsilon_x^0 \\ \varepsilon_y^0 \\ \gamma_{xy}^0 \\ \kappa_x \\ \kappa_y \\ \kappa_{xy} \end{bmatrix}$$

For transversely isotropic material, a set of material properties in direction 1 and one set in either direction 2 or 3 are required. CLT initially calculates a stiffness matrix (Q and $\bar{Q}$) for each lamina with the elastic properties related to the orientation of the fibers. Hence, $\bar{Q}$ signifies all off-axis layers, the ones with fibers on an angle to horizontal axis in global coordination system. Q refers to the stiffness matrix in which the ones with fibers parallel to horizontal axis in global coordination system. Subscript (k) is utilized to tell apart among the different stiffness matrices in each layer i.e. the k^{th} lamina in the laminate.

References

1. Ravishankar, S. and C. Murthy. *Ultrasonic imaging for evaluation of drill-induced delaminations in composite laminates*. in *Proceedings of the 14th World Conference Nondestructive Test*. 1996.
2. Rawat, S. and H. Attia, *Wear mechanisms and tool life management of WC–Co drills during dry high speed drilling of woven carbon fibre composites.* Wear, 2009. **267**(5-8): p. 1022-1030.
3. Saleem, M., L. Toubal, R. Zitoune, and H. Bougherara, *Investigating the effect of machining processes on the mechanical behavior of composite plates with circular holes.* Composites Part A: Applied Science and Manufacturing, 2013. **55**: p. 169-177.
4. Brinksmeier, E., S. Fangmann, and R. Rentsch, *Drilling of composites and resulting surface integrity.* CIRP annals, 2011. **60**(1): p. 57-60.
5. Ho-Cheng, H. and C. Dharan, *Delamination during drilling in composite laminates.* 1990.
6. Tsao, C., H. Hocheng, and Y. Chen, *Delamination reduction in drilling composite materials by active backup force.* CIRP annals, 2012. **61**(1): p. 91-94.
7. Hocheng, H., C. Tsao, C. Liu, and H. Chen, *Reducing drilling-induced delamination in composite tube by magnetic colloid back-up.* CIRP Annals, 2014. **63**(1): p. 85-88.
8. Suresh, N., S. Ganesh, and T. Jagadesh, *Investigations into edge radius and point angle on energy consumption during micro drilling of titanium alloy.* Materials Today: Proceedings, 2020.
9. Zhang, A., C. Bian, X. Zhang, J. Zhang, Z. Liu, and S. Zhang, *Effect of feed condition on thrust force and torque during continuous and step-by-step drilling of cortical bone.* Procedia CIRP, 2020. **89**: p. 201-206.
10. Kumar, J., R.K. Verma, and K. Debnath, *A new approach to control the delamination and thrust force during drilling of polymer nanocomposites reinforced by graphene oxide/carbon fiber.* Composite Structures, 2020. **253**: p. 112786.
11. Mudhukrishnan, M., P. Hariharan, and K. Palanikumar, *Measurement and analysis of thrust force and delamination in drilling glass fiber reinforced polypropylene composites using different drills.* Measurement, 2020. **149**: p. 106973.
12. Khanna, N., F. Pusavec, C. Agrawal, and G.M. Krolczyk, *Measurement and evaluation of hole attributes for drilling CFRP composites using an indigenously developed cryogenic machining facility.* Measurement, 2020. **154**: p. 107504.
13. Upputuri, H.B., V.S. Nimmagadda, and E. Duraisamy, *Optimization of drilling parameters on carbon fiber reinforced polymer composites using fuzzy logic.* Materials Today: Proceedings, 2020. **23**: p. 528-535.
14. Nagaraj, A., A. Uysal, and I. Jawahir, *An Investigation of Process Performance when Drilling Carbon Fiber Reinforced Polymer (CFRP) Composite under Dry, Cryogenic and MQL Environments.* Procedia Manufacturing, 2020. **43**: p. 551-558.
15. Strong, A.B., *Fundamentals of composites manufacturing: materials, methods and applications*. 2008: Society of Manufacturing Engineers.
16. da Costa, R., *Modeling of Fiber Kinking in Composite Laminates.* 2015.

17. Sackey, S.M. and S. Owusu-Ofori. *A dynamic modeling technique for damage progression in drilling of composite laminates*. in *Papers Presented at NAMRC 32*. 2004.
18. Madhavan, V., G. Lipczynski, B. Lane, and E. Whitenton, *Fiber orientation angle effects in machining of unidirectional CFRP laminated composites.* Journal of Manufacturing Processes, 2015. **20**: p. 431-442.
19. Langella, A., L. Nele, and A. Maio, *A torque and thrust prediction model for drilling of composite materials.* Composites Part A: Applied Science and Manufacturing, 2005. **36**(1): p. 83-93.
20. Seeholzer, L., D. Scheuner, and K. Wegener, *Analytical force model for drilling out unidirectional carbon fibre reinforced polymers (CFRP).* Journal of Materials Processing Technology, 2020. **278**: p. 116489.
21. Teti, R., *Machining of composite materials.* CIRP Annals, 2002. **51**(2): p. 611-634.
22. Dandekar, C.R. and Y.C. Shin, *Modeling of machining of composite materials: a review.* International Journal of Machine tools and manufacture, 2012. **57**: p. 102-121.
23. Liu, D., Y. Tang, and W. Cong, *A review of mechanical drilling for composite laminates.* Composite structures, 2012. **94**(4): p. 1265-1279.
24. Higuchi, R., S. Warabi, W. Ishibashi, and T. Okabe, *Experimental and numerical investigations on push-out delamination in drilling of composite laminates.* Composites Science and Technology, 2020. **198**: p. 108238.
25. Phadnis, V., A. Roy, and V. Silberschmidt. *Finite element analysis of drilling in carbon fiber reinforced polymer composites*. in *Journal of Physics-Conference Series*. 2012.
26. Feito, N., J. López-Puente, C. Santiuste, and M. Miguélez, *Numerical prediction of delamination in CFRP drilling.* Composite Structures, 2014. **108**: p. 677-683.
27. Isbilir, O. and E. Ghassemieh, *Numerical investigation of the effects of drill geometry on drilling induced delamination of carbon fiber reinforced composites.* Composite Structures, 2013. **105**: p. 126-133.
28. Phadnis, V.A., A. Roy, and V.V. Silberschmidt, *A finite element model of ultrasonically assisted drilling in carbon/epoxy composites.* Procedia Cirp, 2013. **8**: p. 141-146.
29. Makhdum, F., V.A. Phadnis, A. Roy, and V.V. Silberschmidt, *Effect of ultrasonically-assisted drilling on carbon-fibre-reinforced plastics.* Journal of Sound and Vibration, 2014. **333**(23): p. 5939-5952.
30. Ullah, H., A.R. Harland, T. Lucas, D. Price, and V.V. Silberschmidt, *Finite-element modelling of bending of CFRP laminates: Multiple delaminations.* Computational Materials Science, 2012. **52**(1): p. 147-156.
31. Cheng, Z., Y. Liu, C. Meng, Y. Dai, L. Luo, and X. Liu, *Constructing a weaving structure for aramid fiber by carbon nanotube-based network to simultaneously improve composites interfacial properties and compressive properties.* Composites Science and Technology, 2019. **182**: p. 107721.
32. Guo, Q., Y. Zhang, R. Guo, M. Ma, and L. Chen, *Influences of weave parameters on the mechanical behavior and fracture mechanisms of multidirectional angle-interlock 3D woven composites.* Materials Today Communications, 2020. **23**: p. 100886.
33. Jain, S. and D. Yang, *Effects of feedrate and chisel edge on delamination in composites drilling.* 1993.

34. Rimpault, X., J.-F. Chatelain, J. Klemberg-Sapieha, and M. Balazinski, *Tool wear and surface quality assessment of CFRP trimming using fractal analyses of the cutting force signals.* CIRP Journal of Manufacturing Science and Technology, 2017. **16**: p. 72-80.
35. Dogrusadik, A. and A. Kentli, *Experimental investigation of support plates' influences on tool wear in micro-drilling of CFRP laminates.* Journal of Manufacturing Processes, 2019. **38**: p. 214-222.
36. Girot, F., F. Dau, and M.E. Gutiérrez-Orrantia, *New analytical model for delamination of CFRP during drilling.* Journal of Materials Processing Technology, 2017. **240**: p. 332-343.
37. Gururaja, S. and M. Ramulu, *Modified exit-ply delamination model for drilling FRPs.* Journal of composite materials, 2009. **43**(5): p. 483-500.
38. Phapale, K., R. Singh, and R. Singh, *Comparative Assessment of Delamination control techniques in Conventional drilling of CFRP.* Procedia Manufacturing, 2020. **48**: p. 123-130.
39. Uhlmann, E., F. Sammler, S. Richarz, G. Reucher, R. Hufschmied, A. Frank, B. Stawiszynski, and F. Protz, *Machining of carbon and glass fibre reinforced composites.* Procedia CIRP, 2016. **46**: p. 63-66.
40. Zitoune, R. and F. Collombet, *Numerical prediction of the thrust force responsible of delamination during the drilling of the long-fibre composite structures.* Composites Part A: Applied Science and Manufacturing, 2007. **38**(3): p. 858-866.
41. Ojo, S.O. and M. Paggi, *A thermo-visco-elastic shear-lag model for the prediction of residual stresses in photovoltaic modules after lamination.* Composite Structures, 2016. **136**: p. 481-492.
42. Ojo, S.O. and M. Paggi, *A 3D coupled thermo-visco-elastic shear-lag formulation for the prediction of residual stresses in photovoltaic modules after lamination.* Composite Structures, 2016. **157**: p. 348-359.
43. Won, M.S. and C. Dharan, *Chisel edge and pilot hole effects in drilling composite laminates.* J. Manuf. Sci. Eng., 2002. **124**(2): p. 242-247.
44. Hahn, H.T. and S.W. Tsai, *Nonlinear elastic behavior of unidirectional composite laminae.* Journal of Composite Materials, 1973. **7**(1): p. 102-118.
45. Boresi, A.P., R.J. Schmidt, and O.M. Sidebottom, *Advanced mechanics of materials*. Vol. 6. 1993: Wiley New York.
46. Ismail, S.O., S.O. Ojo, and H.N. Dhakal, *Thermo-mechanical modelling of FRP cross-ply composite laminates drilling: Delamination damage analysis.* Composites Part B: Engineering, 2017. **108**: p. 45-52.
47. Madenci, E. and R. Westman, *Local delamination buckling in layered composites*. 1987, Ph. D. dissertation, MANE department, UCLA.
48. Vizzini, A.J. and P.A. Lagace, *The buckling of a delaminated sublaminate on an elastic foundation.* Journal of composite materials, 1987. **21**(12): p. 1106-1117.
49. Benzeggagh, M.L. and M. Kenane, *Measurement of mixed-mode delamination fracture toughness of unidirectional glass/epoxy composites with mixed-mode bending apparatus.* Composites science and technology, 1996. **56**(4): p. 439-449.
50. Timoshenko, S.P. and S. Woinowsky-Krieger, *Theory of plates and shells*. 1959: McGraw-hill.
51. Lachaud, F., R. Piquet, F. Collombet, and L. Surcin, *Drilling of composite structures.* Composite structures, 2001. **52**(3-4): p. 511-516.

52. Lachaud, F., R. Piquet, and L. Michel. *Delamination in mode I and II of carbon fibre composite materials: fibre orientation influence*. in *Proc. 12th International Conference on Composite Materials, Paris, July*. 1999.
53. Slayton, R. and G. Spinardi, *Radical innovation in scaling up: Boeing's Dreamliner and the challenge of socio-technical transitions.* Technovation, 2016. **47**: p. 47-58.
54. Singh, I., N. Bhatnagar, and P. Viswanath, *Drilling of uni-directional glass fiber reinforced plastics: experimental and finite element study.* Materials & Design, 2008. **29**(2): p. 546-553.
55. Phadnis, V.A., F. Makhdum, A. Roy, and V.V. Silberschmidt, *Drilling in carbon/epoxy composites: experimental investigations and finite element implementation.* Composites Part A: Applied Science and Manufacturing, 2013. **47**: p. 41-51.
56. Durão, L., M. De Moura, and A. Marques, *Numerical prediction of delamination onset in carbon/epoxy composites drilling.* Engineering Fracture Mechanics, 2008. **75**(9): p. 2767-2778.
57. Wang, D., X. He, Z. Xu, W. Jiao, F. Yang, L. Jiang, L. Li, W. Liu, and R. Wang, *Study on damage evaluation and machinability of UD-CFRP for the orthogonal cutting operation using scanning acoustic microscopy and the finite element method.* Materials, 2017. **10**(2): p. 204.
58. Van Luttervelt, C., T. Childs, I. Jawahir, F. Klocke, P. Venuvinod, Y. Altintas, E. Armarego, D. Dornfeld, I. Grabec, and J. Leopold, *Present situation and future trends in modelling of machining operations progress report of the CIRP Working Group 'Modelling of Machining Operations'.* CIRP Annals, 1998. **47**(2): p. 587-626.
59. Mahdi, M. and L. Zhang, *A finite element model for the orthogonal cutting of fiber-reinforced composite materials.* Journal of materials processing technology, 2001. **113**(1-3): p. 373-377.
60. Hashin, Z. and A. Rotem, *A fatigue failure criterion for fiber reinforced materials.* Journal of composite materials, 1973. **7**(4): p. 448-464.
61. Puck, A., *Festigkeitsanalyse von Faser-Matrix-Laminaten: Modelle für die Praxis*. 1996: Hanser.
62. Wang, G.D., N. Li, S.K. Melly, T. Peng, Y. chi Li, Q. Di Zhao, and S. De Ji, *Monitoring the drilling process of GFRP laminates with carbon nanotube buckypaper sensor.* Composite Structures, 2019. **208**: p. 114-126.
63. Wang, G.-D. and S.K. Melly, *Three-dimensional finite element modeling of drilling CFRP composites using Abaqus/CAE: a review.* The International Journal of Advanced Manufacturing Technology, 2018. **94**(1): p. 599-614.
64. Gilpin, A., *Tool solutions for machining composites.* Reinforced plastics, 2009. **53**(6): p. 30-33.
65. Khashaba, U., *Drilling of polymer matrix composites: a review.* Journal of composite materials, 2013. **47**(15): p. 1817-1832.
66. Luo, B., Y. Li, K. Zhang, H. Cheng, and S. Liu, *Effect of workpiece stiffness on thrust force and delamination in drilling thin composite laminates.* Journal of Composite Materials, 2016. **50**(5): p. 617-625.
67. Massoom, Z.F. and H. Kishawy, *Prediction of critical thrust force generated at the onset of delamination in machining carbon reinforced composites.* The International Journal of Advanced Manufacturing Technology, 2019. **103**(5-8): p. 2751-2759.
68. Barbero, E.J., *Introduction to composite materials design*. 2017: CRC press.

69. Chou, T.-W., *Microstructural design of fiber composites*. 2005: Cambridge University Press.
70. Shaw, M.C. and J. Cookson, *Metal cutting principles*. Vol. 2. 2005: Oxford university press New York.